Gut IgA enhances systemic IgG responses to pneumococcal vaccines through the commensal microbiota

Authors: Cindy Gutzeit,[1†] Emilie K. Grasset,[1,2†*] Dean B. Matthews,[1‡] Paul J. Maglione,[3‡] Graham J. Britton,[4] Haley Miller,[1] Giuliana Magri,[5] Lewis Tomalin,[6] Matthew Stapylton,[6] Marc Pybus,[7] Sonia Tejedor Vaquero,[5] Lin Radigan,[13] Roser Tachó-Piñot,[5] Mauricio Guzman,[5] Andrea Martín Nalda,[8,9,10] Marina García Prat,[8,9,10] Monica Martinez Gallo,[9,11] Romina Dieli-Crimi,[11] José C. Clemente,[1,6] Saurabh Mehandru,[1,12] Mayte Suarez-Farina,[6] Jeremiah J. Faith,[1,12] Charlotte Cunningham-Rundles,[13]Andrea Cerutti[1,5,14,15*]

Affiliations:

[1]Department of Medicine, Precision Immunology Institute, Icahn School of Medicine at Mount Sinai; New York, NY 10029, USA.

[2]Department of Pediatrics, Weill Cornell Medicine; New York, NY 10021, USA.

[3]Pulmonary Center and Department of Medicine, Boston University; Boston, MA.

[4]Precision Immunology Institute, Icahn Institute for Data Science and Genome Technology, School of Medicine at Mount Sinai; New York, NY 10029, USA.

[5]Program for Inflammatory and Cardiovascular Disorders, Institute Hospital del Mar for Medical Investigations (IMIM); 08003 Barcelona, Spain.

[6]Department of Genetics and Genomic Sciences, Icahn Institute for Genomics & Multiscale Biology, Icahn School of Medicine at Mount Sinai; New York, NY 10029, USA.

[7]Molecular Biology Laboratory, Fundació Puigvert, Instituto de Investigaciones Biomédicas Sant Pau (IIB-Sant Pau); 02041 Barcelona, Spain.

[8]Infection in Immunocompromised Pediatric Patients Research Group, Vall d'Hebron Institut de Recerca (VHIR), Vall d'Hebron University Hospital (HUVH), Vall d'Hebron Barcelona Hospital Campus; 08035 Barcelona, Spain.

[9]Pediatric Infectious Diseases and Immunodeficiencies Unit, Vall d'Hebron University Hospital (HUVH), Barcelona Autònoma University (UAB); 48201 Barcelona, Spain.

[10]Jeffrey Modell Diagnostic and Research Center for Primary Immunodeficiencies; 08035 Barcelona, Spain.

[11]Division of Immunology, Vall d'Hebron University Hospital (HUVH), Barcelona Autònoma University (UAB); 48201 Barcelona, Spain.

[12]Department of Gastroenterology, Precision Immunology Institute, Icahn School of Medicine at Mount Sinai; New York, NY 10029, USA.
[13]Departments of Medicine and Pediatrics, Precision Immunology Institute, Icahn School of Medicine at Mount Sinai; New York, NY 10029, USA.
[14]Catalan Institute for Research and Advanced Studies (ICREA); 08003 Barcelona, Spain.
[†,‡]These authors contributed equally to this work.
[*]Correspondence to emg4011@med.cornell.edu (E.K.G.) or acerutti@imim.es (A.C.)

Abstract: The gut microbiota enhances systemic immunoglobulin G (IgG) responses to vaccines, but it is unknown whether this effect involves IgA, an antibody that coats intestinal microbes. That IgA may amplify antigen-specific IgG production is suggested by the impairment of IgG responses to pneumococcal vaccines in some IgA-deficient patients. Here we found that anti-pneumococcal but not total IgG production was impaired in mice with global or intraluminal IgA deficiency. The positive effect of gut IgA on anti-pneumococcal IgG responses implicated gut bacteria, as these responses were attenuated in germ-free recipient mice recolonized with gut microbes from IgA-deficient donors. IgA exerted this effect by constraining the systemic translocation of gut commensal antigens, which caused chronic immune activation, including T cell overexpression of programmed cell death-1 (PD-1). This immune inhibitory receptor hindered anti-pneumococcal IgG production by mitigating B cell functionality, which improved upon anti-PD-1 treatment. Thus, gut IgA is functionally linked to systemic IgG via gut microbes.

One sentence Summary: Gut IgA enhances systemic IgG responses to pneumococcal vaccines by constraining microbiota-driven hyperactivation of the immune system.

Main Text:

INTRODUCTION

The intestinal mucosa includes commensal bacteria, fungi, viruses and other microbial and eukaryotic species collectively referred to as microbiota, which modulates host immunity, metabolism and neuronal signaling (*1–3*). The gut microbiota also modulates inflammatory, autoimmune and allergic disorders (*4–6*) as well as the outcome of immune interventions such as vaccination and cancer therapy (*7*, *8*), including treatment with checkpoint inhibitors of the programmed death-1 (PD-1) receptor (*9*). While these studies have mostly focused on the microbial component of the gut microbiota, this "prokaryotic organ" of our body further includes immunoglobulin A (IgA), a microbe-binding mucosal antibody produced by intestinal B cells (*10*). Yet, the role of gut IgA in systemic immunity remains unknown.

IgA mostly derives from intestinal B cell responses to commensal bacteria, which function as major IgA inducers (*10*). These responses occur under homeostatic conditions through complementary T cell-dependent (TD) and T cell-independent (TI) pathways that yield distinct pools of IgA antibodies (*11*, *12*). Conversely, IgA interaction with gut commensals shapes the topography, composition and immunometabolic properties of the intestinal microbiota (*13*). However, the impact of gut IgA on systemic IgG responses remains elusive.

Growing evidence indicates that IgA cooperates with IgG to enhance protection against both commensals and pathogens (*14–16*). Accordingly, some patients with IgA deficiency (IGAD) develop mucosal infections in addition to gut dysbiosis (*17–20*). Of note, infections by common lung pathogens such as *Streptococcus pneumoniae* are usually controlled by IgG (*10*), which can be readily elicited by pneumococcal vaccines (*21*). Remarkably, some IGAD patients with

heterogeneous phenotypic traits show impaired systemic IgG responses to pneumococcal vaccines (*22*, *23*). In addition, some IGAD patients exhibit a concomitant IgG subclass deficiency, whereas others develop a global and profound IgG depletion as they progress to common variable immunodeficiency (*24*). Altogether, these observations suggest that IgA may be more functionally connected to IgG than commonly thought.

Accordingly, the IgA-targeted motility protein flagellin from gut microbes enhances IgG responses to an influenza vaccine in addition to promoting IgA production (*25*, *26*). Similarly, gut microbial metabolites amplify IgG in addition to IgA responses (*27*). Furthermore, immune adaptations to the microbiota, including IgA production, limit the potentially harmful host tissue response caused by unrestrained penetration of gut metabolites into tissues (*28*). Notwithstanding this evidence, whether intestinal IgA influences systemic IgG production remains unknown.

Here we report that IgG responses to pneumococcal vaccines were impaired in IgA-deficient mice. This impairment involved the gut microbiota, because it could be partly recapitulated in ex-germfree (GF) recipient mice recolonized with gut microbes from IgA-deficient mouse donors. IgA-deficient mice showed B cell hyper-activation and grossly augmented IgG responses to gut commensal antigens, presumably due to the enhanced systemic penetration of these antigens. The concomitant T cell hyper-activation started early in life and increased PD-1 expression, which interfered with vaccine-induced IgG production but ameliorated upon anti-PD-1 treatment. These data unveil a hitherto unknown functional link between IgA and IgG.

RESULTS

IgA enhances IgG responses to TI immunogens

The human vaccine Pneumovax23 includes unconjugated pneumococcal polysaccharides (PPS)

from 23 highly pathogenic serotypes of *Streptococcus pneumoniae* (*21*). PPS induce IgG by activating splenic marginal zone (MZ) B cells in a TI manner, as opposed to microbial proteins that activate follicular (FO) B cells in a TD manner (*21*, *29*). First, we determined systemic IgG responses to Pneumovax23 in IgA-deficient C57BL/6 *Igha*$^{-/-}$ mice. These mice were generated by deleting the Iα exon, which initiates germline transcription of both switch α region and constant α gene; the intronic switch α region, which guides class switching from IgM to IgA; and the 5' half of the constant α gene, which encodes the constant α region of IgA (*30*). Wild type (WT) and *Igha*$^{-/-}$ breeders were set up from heterozygous *Igha*$^{+/-}$ parents to control for microbiota and genetic background variability between strains. WT mice used came from these breeders, unless indicated otherwise.

Enzyme-linked immunosorbent assay (ELISA) showed that, compared to WT controls, *Igha*$^{-/-}$ mice did not induce serum IgG3 to PPS at 3 and 7 days following intravenous (i.v.) immunization with Pneumovax23 (**Fig. 1 A**). Together with IgG3, IgM is a major component of humoral immunity to TI antigens (*29*) and *Igha*$^{-/-}$ mice produced more PPS-specific IgM both at baseline and after Pneumovax23 immunization compared to WT controls (**Fig. 1 A**). Like Pneumovax23, replication-incompetent *Streptococcus pneumoniae* induced less specific IgG3 but more specific IgM in *Igha*$^{-/-}$ mice at day 7 following i.v. immunization (**Fig. S1 A**).

Next, we ascertained whether IgA deficiency impaired IgG3 responses to TI antigens different from unconjugated PPS. Compared to WT controls, *Igha*$^{-/-}$ mice showed no 2,4,6-trinitrophenyl (TNP)-specific IgG3 but increased TNP-specific IgM at steady state and 3 or 5 days following i.v. immunization with TNP-Ficoll (**Fig. 1 B**), a haptenated polysaccharide structurally mimicking native PPS. While TNP-Ficoll activates MZ and B-1 B cells by crosslinking the B

cell antigen receptor (BCR), TNP-lipopolysaccharide (LPS) activates MZ and B-1 B cells by co-engaging Toll-like receptor 4 (TLR4) and BCR (*31*). Compared to WT controls, *Igha*$^{-/-}$ mice induced less TNP-specific IgG3 but more TNP-specific IgM 3 and 7 days following i.v. immunization with TNP-LPS (**Fig. S1 B**). We then wondered whether IgA deficiency globally impaired IgG3 production. Total serum IgG3 was readily detectable in *Igha*$^{-/-}$ mice, although less compared to WT controls (**Fig. 1 C**). This finding ruled out a global impairment of IgM-to-IgG3 class switching and IgG3 secretion in B cells from *Igha*$^{-/-}$ mice. As reported earlier (*30*), these mice also showed more total serum IgM compared to WT controls (**Fig. 1 C**), which implied that IgA deficiency was not associated with a general impairment of B cell activation.

We next wondered whether IgA deficiency caused MZ B cell depletion (*29*), but flow cytometry showed more splenic MZ B cells in *Igha*$^{-/-}$ mice compared to WT controls (**Fig. 1 D** and **1 E**). We also determined whether IgA deficiency impaired IgG3 class switching and plasma cell (PC) differentiation in response to commonly used TI antigens. Compared to WT controls, splenic IgG3 class-switched B cells increased 5 days following i.v. immunization of *Igha*$^{-/-}$ mice with TNP-Ficoll, whereas IgG3 class-switched plasmablasts and PCs decreased (**Figure 1 F** and **1 G**). This decrease was not due to an intrinsic B cell defect, as splenic B cells from WT and *Igha*$^{-/-}$ mice cultured with the TI antigen LPS for 4 days comparably differentiated to plasmablasts (**Fig. S1 C** and **S1 D**). Thus, IgA enhances systemic IgG responses to TI immunogens through a B cell extrinsic mechanism involving PC differentiation and/or survival.

IgA augments IgG responses to TD immunogens

Next, we determined whether IgA deficiency impaired systemic IgG responses to the TD conjugated pneumococcal vaccine Prevnar13, which encompasses protein-conjugated PPS from 13 highly pathogenic serotypes of *Streptococcus pneumoniae* (*21*). Compared to WT controls,

Igha$^{-/-}$ mice induced less IgG1 to PPS from the Prevnar13 vaccine 7 and 28 days following i.v. immunization (**Fig. 2 A**). However, this decrease was not associated with gross quantitative alterations of splenic IgG1 class-switched B cell, plasmablasts and PCs (**Fig. 2 B** and **Fig. S2 A**). We then verified whether IgA deficiency impaired the magnitude and affinity of systemic IgG1 responses to 4-hydroxy-3-nitrophenyl-ovalbumin (NP-OVA), a commonly used TD immunogen. Compared to WT controls, *Igha*$^{-/-}$ mice induced less IgG1 with either high (NP7) or low (NP23) affinity 7, 14, 21, 28 or 62 days following i.p. immunization with NP-OVA and alum (**Fig. 2 C** and **Fig. S2 B**). In immunized *Igha*$^{-/-}$ mice, the reduction of IgG1 affinity maturation was most evident at day 7 and 14 and remained significant up to day 28 (**Fig. 2 D**).

We also wondered whether IgA deficiency depleted FO B cell precursors of IgG1-secreting cells and found that the absolute number but not the frequency of these cells was increased in *Igha*$^{-/-}$ mice compared to WT controls (**Fig. 2 E** and **2 F**). We further evaluated whether IgA deficiency caused B cell-intrinsic alterations of TD-induced IgG1 class switching and secretion. Splenic B cells from *Igha*$^{-/-}$ mice induced surface IgG1 expression, PC differentiation, and IgG1 secretion as much as splenic B cells from WT controls upon incubation for 6 days with an agonistic antibody to CD40 mimicking CD40 ligand (CD40L) and interleukin-4 (IL-4) (**Fig. 2 G**-**K**).

Finally, we determined whether IgA deficiency altered splenic T cells and dendritic cells (DCs), which are essential for FO B cells to initiate TD antibody responses (*32*). Compared to WT controls, *Igha*$^{-/-}$ mice showed overlapping frequencies and absolute numbers of total T cells as well as CD4^{+}, CD8^{+} or CD4^{-}CD8^{-} T cell subsets, except that the frequency of CD4^{-}CD8^{-} T cells was slightly decreased and the absolute number of CD4^{+} T cells was slightly increased (**Fig. S2 C**). Compared to WT controls, *Igha*$^{-/-}$ mice also showed overlapping frequencies and absolute numbers of total DCs as well as CD4^{+}CD8^{-}, CD4^{-}CD8^{+} or CD4^{-}CD8^{-} DC subsets (**Fig.**

S2 D). Thus, IgA may enhance systemic IgG responses to TD immunogens through a B cell-extrinsic mechanism that could operate upstream of PC differentiation.

IgA restrains IgG responses to gut commensal antigens

Next, we evaluated the effect of IgA on steady-state IgG1 production. Consistent with an earlier study (*30*), total serum IgG1 was increased in *Igha*$^{-/-}$ mice compared to WT controls (**Fig. 3 A**), which demonstrated that IgG1 production was not globally impaired in *Igha*$^{-/-}$ mice. Given that IgA limits the penetration of gut commensal bacteria (*10*), we also ascertained whether IgA deficiency increased the systemic IgG1 response to soluble microbial antigens. Compared to WT controls, *Igha*$^{-/-}$ mice showed more serum IgG1 to lipoteichoic acid (LTA) from *Staphylococcus aureus*, CPS14 from *Streptococcus pneumoniae,* LPS from *Salmonella typhimurium* as well as CPS9 from *Streptococcus pneumoniae* (**Fig. 3 C** and **Fig. S3 A**).

Then, we further determined whether IgA deficiency increased peripheral IgG1 responses to gut microbiota antigens. ELISA showed that, compared to WT controls, *Igha*$^{-/-}$ mice had increased serum IgG1 but also IgM to gut bacteria from both SI and colon (**Fig. 3 C** and **3 D**, **Fig. S3 B** and **Fig. S3 C**). The increased serum IgG1 in *Igha*$^{-/-}$ mice reacted to total antigens or surface only antigens from whole bacteria. Lastly, we explored gut IgG1 and IgM responses. Similar to an earlier study (*30*), *Igha*$^{-/-}$ mice showed increased total IgG1 and IgM in feces from both small intestine and colon compared to WT controls (**Fig. S3 D** and **S3 E**). Given that gut IgG usually increases as a result of inflammation (*33*, *34*), we microscopically analyzed the intestinal mucosa from *Igha*$^{-/-}$ mice, which was found to be histologically normal (**Fig. S3 F, Table S1**).

Having shown that IgA deficiency abnormally increased IgG1 production to gut commensal antigens, we evaluated whether this finding stemmed from augmented bacterial breaching of the

intestinal barrier. Similar to mesenteric adipose tissue (MAT) from patients with Crohn's disease (*35*), MAT but not mesenteric lymph nodes (MLNs), liver, or spleen from *Igha*$^{-/-}$ mice yielded more colony-forming units (CFUs) upon incubation on agar plates placed in an anaerobic chamber compared to WT controls (**Fig. 3 E** and **Fig. S3 G**). In line with *Lactobacillus* being normally highly coated with IgA (*36*), mass spectrometry showed increased *Lactobacillus* (*L.*), including *L. murinus*, *L. reuteri* and *L. intestinalis*, in the MAT from *Igha*$^{-/-}$ mice (**Fig. 3 F** and **Fig. S3 H**). Consistent with the possibility that IgA deficiency enhances the systemic penetration of gut commensal antigens, quantitative PCR detected an increased proportion of 16S bacterial DNA in the liver from *Igha*$^{-/-}$ mice, although this increase did not reach statistical. significance (**Fig. S3 I**). Bacterial DNA was comparable in the spleen or MLNs from *Igha*$^{-/-}$ mice (**Fig. S3 I**).

Aside from documenting stool expansion of *Lactobacillus*, 16S ribosomal DNA (rDNA) gene sequencing of the gut microbiota showed that, compared to control *Igha*$^{+/+}$ littermates, co-housed *Igha*$^{-/-}$ mice generated from heterozygous *Igha*$^{+/-}$ parents displayed a depletion of *Lachnospiraceae* (**Fig. 3 G**), some of which are central to homeostatic gut IgA responses and get depleted in IGAD patients (*10, 19, 37, 38*). Thus, besides modulating the abundance of gut IgA-inducing bacteria, gut IgA may optimize systemic IgG responses by constraining the penetration of commensal antigens.

IgA amplifies IgG responses to vaccines via gut commensals

Next, we asked whether the selective lack of mucosal secretory IgA (SIgA) could phenocopy global IgA deficiency. Gut SIgA is absent in *Pigr*$^{-/-}$ mice, which lack the polymeric Ig receptor (pIgR) needed to transport dimeric IgA across intestinal epithelial cells (*10, 39*). Similar to *Igha*$^{-/-}$ mice, *Pigr*$^{-/-}$ mice induced less serum IgG1 to PPS from the Prevnar13 vaccine 21 and 28 days following i.p. immunization compared to WT controls (**Fig. 3 H**). Next, we tested

whether lateral transmission of IgA-coated gut commensals restored anti-pneumococcal IgG responses in *Igha*$^{-/-}$ mice. Compared to control *Igha*$^{+/+}$ littermates, co-housed *Igha*$^{-/-}$ mice generated from heterozygous *Igha*$^{+/-}$ parents still mounted a weaker IgG3 response to PPS from Pneumovax23 7, 14, 21 and 28 days following i.p. immunization (**Fig. S3 J**). Moreover, co-housed *Igha*$^{-/-}$ mice mounted a weaker serum IgG1 response to PPS from Prevnar13 21 and 28 days following i.p. immunization compared to control *Igha*$^{+/+}$ littermates (**Fig. 4 I**).

Considering that mucosa lumen-restricted IgA deficiency was sufficient to decrease systemic IgG responses to PPS and knowing the IgA shapes the composition and function of the intestinal microbiota, we determined whether gut bacteria from *Igha*$^{-/-}$ mice had a negative impact on their anti-pneumococcal IgG response. Compared to ex-GF mice obtained by reconstituting GF recipients with fecal bacteria from WT mice, ex-GF mice obtained by reconstituting GF recipients with fecal bacteria from *Igha*$^{-/-}$ mice induced less IgG1 to PPS 28 days following i.p. immunization with Prevnar13 (**Fig. 3 J**). Thus, IgA may enhance systemic IgG responses to pneumococcal vaccines through mechanisms involving the commensal microbiota.

IgA controls FO B cell differentiation to PCs

Considering the importance of T follicular helper (T_{FH}) cells in B cell activation and IgG1 production (*32*), we explored whether germinal centers (GCs) from gut-associated Peyer's patches, MLNs and spleen of *Igha*$^{-/-}$ mice showed any B cell and/or T cell anomalies. Compared to WT controls, *Igha*$^{-/-}$ mice showed enlarged Peyer's patches and MLNs but normally sized spleen upon macroscopic analysis (**Fig. 4 A** and **Fig. S4 A**). Accordingly, Peyer's patches and MLNs from *Igha*$^{-/-}$ mice had an increased cellularity, while the spleen did not (**Fig. 4 B**). However, flow cytometry detected increased GC B cells and T_{FH} cells not only in Peyer's patches and MLNs, but also in the spleen from *Igha*$^{-/-}$ mice (**Fig. 4 C-F**).

Given that IgA deficiency caused an expansion of GC B cells in splenic follicles from *Igha*$^{-/-}$ mice, we characterized the global transcriptome of splenic FO cells from these mice. This study also included splenic MZ B cells, as IgA deficiency impaired IgG responses to both TD and TI pneumococcal vaccines. RNA-sequencing (RNA-seq) data visualized through volcano plots showed that FO B cells from *Igha*$^{-/-}$ mice had more differentially expressed genes than MZ B cells did when compared to WT controls (**Fig. 4 G**). In addition, gene set variation analysis (GSVA) showed that, compared to WT controls, FO B cells from *Igha*$^{-/-}$ mice expressed more gene sets linked to B cell proliferation, GC differentiation and PC differentiation (**Fig. 4 H**).

As shown by heat maps of RNA-seq data (**Fig. 4 I**), these increased gene sets included transcripts described by a recent study (*40*) and implicated in GC differentiation (e.g., *Tmem121, 2510009E07Rik, Troap, Ncapg, Fscn1*), and PC differentiation (e.g., *Ncapg, Ccna2, Shcbp1*). Having shown that *Igha*$^{-/-}$ mice have enhanced IgG1 responses to commensal antigens, we compared IgG1 class-switched B cells (SBCs) as well as IgG1-expressing PBs and PCs from in *Igha*$^{-/-}$ mice and WT controls. By using a flow cytometric assay capable of distinguishing surface from intracellular IgG1, we determined that *Igha*$^{-/-}$ mice had more IgG1^{+} SBCs, IgG1^{+} PBs, and IgG1^{+} PCs in the spleen as well as MLNs and PPs compared to WT controls (**Fig. 4 J** and **Fig. S4 B** and **S4 C**).

Knowing that IgA starts influencing the intestinal microbiota soon after birth and that gut bacteria stimulate early post-natal immune development (*41, 42*), we determined whether IgA deficiency caused early immune anomalies. We found that both size and cellularity of MLNs were already increased in 5 week-old *Igha*$^{-/-}$ mice compared to WT controls (**Fig. S4 D**). Similar to adult mice, MLNs and spleen from 5 week-old *Igha*$^{-/-}$ mice included more total GC B cells, IgG1^{+} GC B cells, T_{FH} cells, IgG1^{+} SBCs, IgG1^{+} PBs, and IgG1^{+} PCs than WT controls (**Fig. S4**

E and **S4 F**). Accordingly, 5 week-old *Igha*$^{-/-}$ mice also had more total serum IgG1 than WT controls and this increase further augmented in 14 week-old *Igha*$^{-/-}$ mice (**Fig. S4 G**). Like adult mice, 5 week-old *Igha*$^{-/-}$ mice further showed more serum IgG1 to colonic gut microbiota than WT controls, but drastically less serum IgG3 to TNP-Ficoll 5 days following i.p. immunization (**Fig. S4 H** and **S4 I**). Thus, gut IgA may enhance systemic IgG responses to vaccines by constraining the differentiation of FO B cells into IgG-secreting PCs via the GC reaction and may start doing so at a very early age.

IgA constrains T cell expression of the immune inhibitor PD-1

Next, we hypothesized that, in the absence of IgA, the early and persistent exposure to systemically translocated gut antigens could impair peripheral IgG responses to vaccines by chronically activating B cells, which could lead to a state of functional B cell hypo-responsiveness similar to B cell anergy (*43*). Before addressing this point, we first wondered whether the FO B cell hyper-activation detected in *Igha*$^{-/-}$ mice was associated with any gut enrichment in pro-inflammatory segmented filamentous bacteria (SFB). Indeed, it has been recently reported that SFB are expanded in the small intestine of *Igha*$^{-/-}$ mice and contribute to its inflammation (*44*). Consistent with our earlier data showing no inflammation in the gut from *Igha*$^{-/-}$ mice, the small intestine, caecum and colon from these mice showed similar SFB abundance as co-housed *Igha*$^{+/+}$ littermate controls (**Fig. S4J**). This result, together with our earlier finding showing a persistently attenuated anti-pneumococcal IgG1 response in ex-GF mice reconstituted with cecal bacteria from *Igha*$^{-/-}$ donors, suggest that SFB are unlikely to be involved in the FO B cell hyper-activation detected in *Igha*$^{-/-}$ mice

Next, we determined whether B cells from *Igha*$^{-/-}$ mice expressed a gene signature consistent with functional hypo-responsiveness. As shown by GSVA, splenic FO but not MZ B cells from

279 *Igha*$^{-/-}$ mice were enriched in B cell anergy genes compared to WT controls (**Fig. 5 B**). A heat
280 map visualization of DEGs selected on the basis of recently published findings (*43*) highlighted
281 *Cenpv, Lef1, Nefh, Fabp5* and *Tgif1* among several other gene products (**Fig. 5 C**). Considering
282 that the activation-induced receptor PD-1 transmits powerful inhibitory signals to activated B
283 cells via PD-1 ligands (*45, 46*), we also evaluated whether IgA deficiency increased PD-1 and
284 PD-ligand 1 (PD-L1) expression on systemic T and B cells, respectively. Compared to WT
285 controls, *Igha*$^{-/-}$ mice showed more PD-1^{+}CD4^{+} and PD-1^{+}CD8^{+} T cells, including antigen-
286 experienced PD-1^{+}CD44^{+}CD4^{+} and PD-1^{+} CD44^{+}CD8^{+} T cells, in spleen and MLNs but not PPs
287 (**Fig. 5 D** and **Fig. S5 A**). Similar to adult *Igha*$^{-/-}$ mice, 5 week-old *Igha*$^{-/-}$ mice had more PD-
288 1^{+}CD4^{+} T cells, including antigen-experienced PD-1^{+}CD44^{+}CD4^{+} T cells, in both spleen and
289 MLNs (**Fig. S5 B**). Finally, splenic MZ and B-1 but not FO B cells from *Igha*$^{-/-}$ mice exhibited
290 increased PD-L1 expression compared to WT controls (**Fig. 5 E**).

291 The involvement of PD-1 in the inhibition of vaccine-induced IgG1 was further evaluated using
292 anti-PD-1. Compared to WT controls, *Igha*$^{-/-}$ mice i.p. immunized with Prevnar13 and treated
293 with a control isotype-matched antibody showed reduced serum IgG1 to PPS at day 56 and 86
294 (**Fig. 5 F**). In contrast, immunized *Igha*$^{-/-}$ mice treated with anti-PD-1 induced as much serum
295 IgG1 to PPS at day 56 and 86 as WT mice treated with a control antibody (**Fig. 5 F**).

296 We also assessed whether IgA deficiency caused increased gut commensal antigens penetration
297 and peripheral B cell anergy also in humans. Flow cytometry showed an increased frequency of
298 phenotypically anergic IgM^{low}CD21^{low} naïve B cells in blood samples from a New York City
299 (NYC) cohort of adult IGAD patients compared to age-matched controls (**Fig. 6 A** and **Table**
300 **S2**). In these patients, the frequency of IgM^{low}CD21^{low} naïve B cells consistently did not exceed
301 about 4% of total B cells. In agreement with the lack of IgA, the frequency of switched memory

B cells was decreased in IGAD patients, whereas the frequency of circulating total, naïve and MZ-like B cells was normal (**Fig. S5 C** and **S5 D**). These findings were replicated in a Barcelona (BCN) cohort of adult IGAD patients, who also showed a lower frequency of IgA^+ PCs (**Fig. S5 E** and **Table S3**). An additional BCN cohort of IGAD pediatric patients similarly showed a decreased frequency of IgA^+ PCs, which was accompanied by an increased frequency of IgG^+ PCs but a normal frequency of switched memory B cells as well as total, naïve, and MZ-like B cells (**Fig. S5 F** and **Table S3**). Thus, similar to *Igha*$^{-/-}$ mice, IGAD patients showed IgA^+ PC depletion combined with an increase of both "anergic" B cells and IgG^+ PCs (*47*, *48*). This last increase echoes the increased circulating IgG1 to gut commensal antigens found in *Igha*$^{-/-}$ mice. Accordingly, IGAD patients from the NYC cohort showed signs of enhanced gut permeability (*19*, *49*), including more circulating soluble CD14 (sCD14), bacterial 16S rDNA, and IgG to LPS from *Escherichia coli* compared to healthy controls (**Fig. 6 B-D**).

Given that gut microbiota-derived metabolites regulate humoral immunity (*27*, *28*, *50*, *51*), we also hypothesized that gut IgA could further enhance systemic IgG responses to pneumococcal vaccines via metabolites. Capillary electrophoresis time-of-flight mass spectrometry (CE-TOFMS) and liquid chromatography time-of-flight mass spectrometry (LC-TOFMS) showed less abundant branched-chain amino acids (BCAAs), such as leucine and isoleucine but not valine, in plasma from the NYC cohort of adult IGAD patients compared to plasma from age-matched healthy controls (**Fig. S6 A** and **S6 B**). Consistent with an earlier study showing that the BCAA transporter CD98 enhances antibody production (*52*), human B cells cultured with a BCAA mix induced more IgG secretion upon activation by CD40L and IL-21 (**Fig. S6 C**).

Although showing non-significant decrease of plasma BCAAs compared to WT controls (**Fig. S6 D**), *Igha*$^{-/-}$ mice showed significant depletion of plasma spermidine (**Fig. S6 E** and **S6 F**),

which is an endogenous polyamine with known IgG-enhancing properties (*53*). In summary, gut IgA may enhance systemic IgG responses to pneumococcal vaccines by preventing the penetration of gut commensal antigens and the ensuing hyper-activation of systemic B cells (**Fig. 6 E**). In addition to limiting B cell inhibitory signals from activation-induced PD-1^+ T cells, IgA might optimize the availability of gut metabolites enhancing IgG production by B cells.

DISCUSSION

We have shown that gut IgA augments systemic IgG responses to pneumococcal vaccines. By increasing the translocation of gut commensal antigens, IgA deficiency enhanced B cell activation and IgG production along with T cell expression of PD-1. Inhibitory signals from PD-1 mitigated pneumococcal vaccine-specific IgG production by B cells, which exhibited gene signatures linked to functional hypo-responsiveness. Thus, IgA is functionally linked to IgG.

The gut microbiota enhances mucosal IgA and systemic IgG responses to a broad spectrum of bacteria (*14*, *16*, *54*, *55*), which leads to the generation of a pre-immune layer of humoral protection against both non-invasive commensals and invasive pathogens (*15*, *26*). This dual function may stem from the cross-reactivity of some immunodominant antigens shared by commensals and pathogens (*15*, *26*). Consistently, patients with combined IgA and IgG deficiency are at increased risk of both systemic infections and gut inflammation (*16*, *18*, *55*).

Gut commensals also sustain specific systemic IgG responses to vaccines (*25*, *56*). Here, we hypothesized that this effect could involve IgA, which extensively coats the gut microbiota (*36*, *37*). Consistent with this hypothesis, systemic IgG responses to pneumococcal vaccines are impaired in some IGAD patients (*22*, *23*). By showing that IgA-deficient *Igha*$^{-/-}$ mice (*30*) had severely impaired IgG responses to pneumococcal vaccines, our findings indicate that gut IgA is

functionally linked to systemic IgG. The link may be provided by the gut commensal microbiota, because pIgR-deficient *Pigr*$^{-/-}$ mice, which selectively lack intraluminal IgA (*39*), were found to mount an attenuated IgG response to a pneumococcal vaccine compared to WT controls. The involvement of gut commensals was further suggested by the finding that GF recipient mice reconstituted with gut bacteria from *Igha*$^{-/-}$ mouse donors made less systemic IgG to vaccines compared to controls reconstituted with gut bacteria from WT mouse donors.

Of note, the phenotype of *Pigr*$^{-/-}$ mice was milder compared to that of *Igha*$^{-/-}$ mice, which could stem from the massively increased dimeric IgA seen in the circulation of *Pigr*$^{-/-}$ mice (*39*). Indeed, due to its inability to translocate across the gut epithelium, dimeric IgA progressively accumulates in the gut lamina propria of *Pigr*$^{-/-}$ mice (*39*). The ensuing increase of circulating dimeric IgA may enhance the clearance of systemically translocated gut commensal antigens in *Pigr*$^{-/-}$ mice compared to *Igha*$^{-/-}$ mice, which completely lack IgA (*30*). By attenuating the chronic hyper-activation and ensuing functional hypo-responsiveness of systemic B cells, this effect could result into a less compromised anti-pneumococcal IgG response in *Pigr*$^{-/-}$ mice.

Compared to *Igha*$^{-/-}$ mice, also GF receipient mice receiving the gut microbiota from *Igha*$^{-/-}$ mouse donors displayed a milder phenotype, possibly because GF mice progressively restore their IgA response following re-colonization. This gradual recovery of IgA production could attenuate the systemic translocation of commensal antigens across the gut epithelium over time upon recolonization. It must be also noted that, compared to the gut mucosa from *Igha*$^{-/-}$ mice, the gut mucosa from recolonized ex-GF mice is exposed to the microbiota from *Igha*$^{-/-}$ mice for a much shorter time, which may reduce gut contact with dysbiotic bacterial communities enriched in IgG-suppressing factors and/or depleted of IgA-and IgG-enhancing factors.

Earlier works explored the impact of the gut microbiota on IgG responses to vaccines (*25*, *56*), but did not evaluate the contribution of IgA bound to intestinal microbes. Yet, this binding shapes both composition and function of gut commensals, including their metabolic properties (*13*, *19*, *57*, *58*). Furthermore, IgA binding to gut bacteria maximizes microbiota diversity, which is critical for optimal IgG responses to vaccines (*13*, *56*, *57*). Moreover, IgA constraints gut microbes to the intestinal lumen, which limits their interaction with the immune system (*10*, *13*).

Consistent with the involvement of IgA in shaping the composition of gut bacterial communities, IgA deficiency enriched the microbiota in *Lactobacillaceae* among other smaller changes. This mild dysbiosis is consistent with published findings (*44*, *59*) and likely reflects compensatory effects brought about by an increased gut IgM production in the IgA-deficient gut (*11*). It must be also noted that small microbiota compositional differences may be associated with more profound microbiota functional changes, including motility changes that which may not be detected by commonly used high-throughout screening approaches such as the 16S rDNA sequencing method used in this study (*60*).

Motility changes could be at the root of the abnormal MAT translocation of *Lactobacillus (L.) murinus*, *L. reuteri* and *L. intestinalis* detected in *Igha*$^{-/-}$ mice. The MAT-specific translocation of viable Lactobacilli may reflect both the role of MAT as gut antigen-entry site and the role of IgA in the containment of commensals within the gut lumen (*13*, *61*). Accordingly, IgA has been shown to heavily coat Lactobacilli (*36*). Of note, MAT-restricted bacterial translocation has also been observed in Crohn's disease and may relate to the swift engulfment of invading commensals by MAT phagocytes (*35*, *62*). Stromal cells and adipocytes would help phagocytes

to impede bacterial dissemination beyond the MAT (*63*), which likely explains our failure to detect viable bacteria in MLNs as well as liver and spleen from *Igha*$^{-/-}$ mice.

Despite preventing MAT-based live bacteria from traveling to MLNs, liver and spleen, phagocytosis would not impede the systemic penetration of soluble commensal antigens. In *Igha*$^{-/-}$ mice, this process could fuel persistent activation of peripheral B cells, which indeed showed vastly augmented differentiation into PBs and PCs that released IgG1 to soluble microbial antigens, such as CPS, LTA and LPS. Of note, increased systemic presence of gut commensal antigens was consistent with the detection of more bacterial 16S rDNA in both liver from *Igha*$^{-/-}$ mice and circulation from IGAD patients.

In both *Igha*$^{-/-}$ mice and IGAD patients, enhanced gut antigen translocation caused overstimulation of intestinal as well as systemic B, T and possibly myeloid cells. Accordingly, both intestinal and systemic B cells from *Igha*$^{-/-}$ mice secreted more IgG1 as well as IgM to commensal antigens. Due to the hyper-activation of FO B cells by these antigens, splenic GC B cells were increased in *Igha*$^{-/-}$ mice along with GC-based T_{FH} cells. These mice also showed more activated T cells expressing PD-1, an immune inhibitory receptor (*45*). When treated with anti-PD, *Igha*$^{-/-}$ mice ameliorated their anti-pneumococcal IgG1 response, which points to the involvement of PD-1 in the hypo-responsiveness of FO B cells to vaccines.

Similar to *Igha*$^{-/-}$mice, IGAD patients showed an increased frequency of functionally exhausted $IgM^{low}CD21^{low}$ B cells. This increase was combined with augmented circulating sCD14, a soluble antigen released by myeloid cells following activation, including the activation induced by translocated commensal antigens (*19*, *49*). Thus, despite causing bacterial translocation largely restricted to the MAT, IgA deficiency would chronically elicit systemic B cell hyper-

activation and hyper-IgG1 production to commensal antigens by increasing the permeability of the intestinal mucosa. Consistent with its capability to initiate antigen-specific IgG responses after intraperitoneal immunization (*64*, *65*), the MAT could be directly involved in the exaggerated commensal-specific IgG1 response of *Igha*$^{-/-}$mice.

At variance with a recently published study (*44*), the *Igha*$^{-/-}$mice from our colony showed no inflammation and no expansion of pro-inflammatory SFB in the small intestine and caecum compared to WT controls. Although showing increased SFB abundance in *Igha*$^{-/-}$mice, the colonic mucosa was histologically normal. By showing that hyper-IgG1 production did not depend on gut inflammation in *Igha*$^{-/-}$mice, these data support our contention that IgA enhances vaccine-specific IgG responses by constraining the B cell activation and the ensuing B cell exhaustion that would result from persistent gut commensal antigen penetration. This last would be ultimately responsible for hyper-IgG1 production. In addition to limiting T cell expression of PD-1, IgA limited the expression of PD-L1 by B cells, as this ligand increased on MZ B cells from *Igha*$^{-/-}$ mice. Unlike FO B cells, MZ B cells did not show transcriptional signatures reflecting abnormal activation. Yet, their increased PD-L1 expression may be central to the initiation of PD-1-mediated inhibitory signals from T cells. Interestingly, the gut microbiota restrains signaling from PD-1 via inosine, a metabolite that modulates T cells through the adenosine A_{2A} receptor (*51*). This finding raises the possibility that IgA constrains PD-1 expression by supporting gut communities of inosine-releasing commensals.

Co-housing experiments showed that lateral transmission of a healthy gut microbiota into *Igha*$^{-/-}$ mice was not sufficient to rescue vaccine-specific IgG responses. Thus, it is plausible that IgA deficiency irreversibly attenuates systemic IgG responses through a process that starts very early in life via vertical transmission of a dominant dysbiotic gut microbiota from the mother to the

offspring. Accordingly, we found increased IgG1 responses to gut commensals as well as impaired IgG3 production to a PPS-mimicking TI immunogen in *Igha*$^{-/-}$ mice as early as 5 weeks after birth. These data echo published findings showing that IgA drives early post-natal gut microbiota changes and that gut microbes stimulate early post-natal immune development (*41*, *42*). In this regard, IgA may function by optimizing gut retention of consortia with broad IgA-inducing properties, including *Lachnospiraceae* A1 (*38*).

Besides facilitating gut adherence of bacteria capable of excluding harmful competitors (*66*), IgA instigates competitive gut colonization by modulating the metabolic profile of certain commensals (*58*). Accordingly, IGAD patients exhibited systemic depletion of branched chain amino acids (BCAAs) (*50*), which augment IgG responses via CD98, a BCAA transporter expressed by activated B cells (*50*, *52*). Along the same lines, we found that BCAAs enhanced IgG release by *in vitro* activated B cells. Although only marginally reducing circulating BCAAs, *Igha*$^{-/-}$ mice showed significantly depleted spermidine, which is another metabolic enhancer of IgG responses (*53*).

A limitation of this study relates to the extensive differences existing between *Igha*$^{-/-}$ mice and IGAD patients. While *Igha*$^{-/-}$ mice have an absolute IgA deficiency, IGAD patients retain minimal amounts of IgA. In addition, *Igha*$^{-/-}$ mice consistently express the same phenotype, whereas IGAD patients range from asymptomatic individuals to patients with mild, moderate or even severe gastrointestinal and, more commonly, respiratory disorders. These individuals are the only IGAD cases considered in our study, because only these cases come to hospital attention. Their analysis was nonetheless helpful to confirm in humans some of the findings obtained in *Igha*$^{-/-}$ mice. Indeed, this is a study on the fundamental biology of gut IgA rather than on the pathogenesis of IGAD.

In summary, we show that gut IgA amplifies systemic IgG responses to pneumococcal vaccines through mechanisms likely involving the gut microbiota. These IgA-dependent mechanisms start operating early in life and include constrained PD-1 expression by T cells. Aside from revealing an unexpected functional link between gut IgA and systemic IgG, our data indicate that gut IgA should be always considered in studies about the impact of gut microbes on systemic immune responses. Our data also support the potential benefit of oral IgA therapy in patients combining IgA depletion with impaired IgG responses to vaccines, including pneumococcal vaccines.

MATERIALS AND METHODS

Study design

This study was designed to dissect the impact of mucosal IgA on systemic IgG responses to human pneumococcal vaccines. Our hypothesis was that mucosal IgA optimized systemic IgG production. This hypothesis was based on the following considerations. First, some immunodeficient patients lacking IgA have a poor IgG response to pneumococcal vaccines. Second, IgA extensively binds to mucosal commensal bacteria, including intestinal microbes, which in turn are thought to positively influence vaccine-induced IgG production. We compared *Igha*$^{-/-}$ or *Pigr*$^{-/-}$ mice with WT controls to evaluate whether and how the lack of total or intraluminal IgA influenced systemic IgG responses to human pneumococcal vaccines. In addition, we studied peripheral IgG responses to vaccines in ex-GF mice recolonized with gut commensal bacteria from *Igha*$^{-/-}$ mice and WT controls or from IGAD patients or healthy donors. Moreover, we combined *ex vivo* high-throughput studies with *in vivo* treatment of mice by a blocking anti-PD-1 antibody to characterize the mechanism by which IgA enhances IgG production to a pneumococcal vaccine.

Most experiments were performed 2-6 times, showed good reproducibility and were summarized by pooling the data from all the experiments. The following were the exceptions. The flow cytometric analysis following TNP-Ficoll immunization (Fig. 1F-G), the GF mice recolonization with gut commensal bacteria from *Igha*$^{-/-}$ and WT mice (Fig. 4I), and anti-bacterial ligand ELISAs (Fig. 3B, S3A), PD-L1 expression flow experiment (Fig. 5E), and RNA-seq analysis of splenic MZ and FO B cells from *Igha*$^{-/-}$ and WT mice were performed once. The mass spectrometry analysis of serum metabolites was also done once. Human sCD14 was measured in one ELISA on serum collected at different time points (Fig. 6B). The 16S rRNA gene sequencing analysis of the microbiota from colon tissue of WT controls and *Igha*$^{-/-}$ mice (Fig. 3G) was performed once in a well-controlled experiment using co-housed littermates. As shown in supplemental figures, immunizations with *S. Pneumoniae* and TNP-LPS, T cell and DC subset analysis, Pneumovax23 immunization of co-housed littermates, and TNP-Ficoll immunization in 5-week-old mice were performed once. Significant outliers in normally distributed data were determined using Grubb's test with an alpha of 0.05 and excluded from analysis.

Human subjects

Blood samples from the NYC cohort were collected from 42 age-and sex-matched HCs and IGAD patients at Icahn School of Medicine at Mount Sinai (**Table S2**). The Institutional Review Board of Icahn School of Medicine at Mount Sinai approved the use of blood and stool specimens. Human blood samples from the BCN cohort were collected from age- and sex-matched HCs and IGAD patients at Vall d'Hebrón Hospital (**Table S3**). The Ethical Committee of Clinical Research of Vall d'Hebrón Hospital approved the use of blood samples.

Analysis of human blood and stool samples

For the phenotypic study of B cells by flow cytometry, blood was collected in sodium-heparin blood collection tubes. Peripheral blood mononuclear cells (PBMCs) were obtained from sodium heparinized blood samples by separation on Ficoll Histopaque-1077 gradient (Sigma-Aldrich). For metabolomics analysis, blood from fasted patients was collected in BD Vacutainer K2EDTA blood collection tubes (Becton Dickinson). Human stool samples from the NYC cohort were collected from HCs and IGAD patients, shipped overnight on ice packs to the laboratory, and immediately stored at -80°C degrees. Human stool samples from the NYC cohort were collected from HCs and IGAD patients, shipped overnight on ice packs to the laboratory, and immediately stored at -80°C degrees. Frozen samples were pulverized under liquid nitrogen in a sterile hood and processed as detailed in Supplementary Materials and Methods.

Mice

C57BL/6J (The Jackson Laboratory), *Igha*$^{-/-}$ (*30*) and *Pigr*$^{-/-}$ mice (*39*) were bred in the animal facility of Icahn School of Medicine at Mount Sinai under specific pathogen free (SPF) conditions. *Igha*$^{-/-}$ mice were obtained from Sergio Lira (Icahn School of Medicine at Mount Sinai), whereas *Pigr*$^{-/-}$ mice were provided by Beth Garvy (University of Kentucky). WT and *Igha*$^{-/-}$ breeders were set up from heterozygous *Igha*$^{+/-}$ parents to control for microbiota and genetic background variability between strains. WT controls used in experiments came from these breeders except where pointed out. Similarly, WT and *Pigr*$^{-/-}$ breeders were set up from heterozygous *Pigr*$^{+/-}$ parents. Both sexes were used and mice were 4-16 weeks old for steady state experiments and 5-12 weeks old for immunization experiments. Since all mouse strains used in this manuscript mounted a specific IgM response upon immunizations, mice lacking induction of specific IgM were excluded from analysis due to presumed poor immunization. All animal experiments described in this study were approved by Institutional Animal Care and Use

Committee (IACUC) of the Icahn School of Medicine at Mount Sinai and were performed in accordance with the approved guidelines for animal experimentation at the Icahn School of Medicine at Mount Sinai. GF C57BL/6J mice were bred in-house at the Mount Sinai Immunology Institute Gnotobiotic Facility in flexible vinyl isolators. To facilitate high-throughput studies in gnotobiotic mice, ‘‘out-of-the-isolator’’ gnotobiotic techniques were utilized (*67*). Shortly after weaning and under strict aseptic conditions, 28-42-days old GF mice were transferred to autoclaved filter-top cages outside of the breeding isolator and colonized with human or murine microbiota.

Analysis of murine blood and stool samples

Murine blood and stool samples were collected and analyzed as detailed in Supplementary Materials and Methods.

Colonization of GF mice

GF mice were reconstituted with fecal bacteria from WT or *Igha*$^{-/-}$ mice and HCs or IGAD patients as detailed in Supplementary Materials and Methods.

Isolation and identification of translocated gut bacteria

Translocated gut bacteria were quantified and identified as detailed in Supplementary Materials and Methods.

Culture of bacteria

Streptococcus pneumoniae was cultured as detailed in Supplementary Materials and Methods.

Immunizations

Each mouse was i.v. or i.p. immunized as detailed in Supplementary Materials and Methods.

Bacteria isolation from mouse feces

Fecal pellets collected directly from mice or from the small intestine were homogenized in PBS (1 ml/0.1 g) by vortexing for 10 minutes at room temperature. Suspension was centrifuged twice at 2,000 rpm for 5 minutes at 4°C and supernatants collected. For bacterial flow cytometry assays, an aliquot was removed from this supernatant. After centrifugation at 8000 g for 10 minutes at 4°C, supernatant was collected to measure free fecal IgM and IgG1. Resulting bacterial pellets were used to determine microbiota-specific IgG1 (see ELISA).

Flow cytometry and cell sorting

1-2 × 10^6 cells per sample were resuspended in PBS with CD16/32 Fc Block (BD Biosciences) and Live/Dead staining (Invitrogen) for 10 minutes on ice. Cells were then washed with FACS buffer (PBS supplemented with 2% heat-inactivated FBS and 2 mM EDTA (Fisher)), and subsequently stained with appropriately diluted antibodies for 30 minutes on ice as detailed in Supplementary Materials and Methods.

ELISA

Total or antigen-specific antibody subclasses, including high-affinity and low-affinity antibodies specific to NP and microbiota-reactive antibodies, as well as IL-4 and sCD14 were quantified as detailed in Supplementary Materials and Methods.

RNA-seq

RNA was extracted from sorted splenic murine MZ and FO B cells using QIAshredder and RNeasy Plus Micro Kit (Qiagen). Library preparation and sequencing were performed by a specialized company (GENEWIZ). RNA-seq analysis was performed as detailed in Supplementary Materials and Methods. RNA-seq sequence data files (fastq) are stored in the public SRA under project number GSE173361 (reviewer token: abizcussbtwtzgh).

16S rRNA gene sequencing and analysis

DNA extraction, library preparation, and 16S rRNA gene amplicon sequencing of colonic fecal bacteria from co-housed littermate WT and *Igha*$^{-/-}$ mice were outsourced (GENEWIZ). 16S sequence data files (fastq) are stored in the public SRA under project number PRJNA722766 (reviewer link: https://dataview.ncbi.nlm.nih.gov/object/PRJNA722766?reviewer=4nf2agqsarp8ni0iaei1flufa).

Metabolomics

Sera were collected from HCs, IGAD patients, SPF WT mice or SPF *Igha*$^{-/-}$ mice as described above. HCs and IGAD patients were asked to fast overnight, and food was withheld from mice overnight prior to collection. Collected serum was frozen at −80°C and shipped to Human Metabolome Technologies for further analysis as detailed in Supplementary Materials and Methods.

Human and mouse B cell cultures

Human and mouse B cells were cultured as detailed in Supplementary Materials and Methods.

Histology and immunofluorescence

Colon and small intestine from WT or *Igha*$^{-/-}$ mice were processed as detailed in Supplementary Materials and Methods.

Statistical analysis

Statistical analysis was performed using Prism version 9.0 (GraphPad). Comparisons between two groups were determined using either Student's t test when data followed a normal distribution or Mann-Whitney U test when data were not normally distributed. Normal/Gaussian distribution was determined by a D'Agostino and Pearson normality test. For multiple comparisons, a Kruskal-Wallis test with Dunn's correction was used. Significant outliers were

592 determined using Grubb's test with an alpha of 0.05 and excluded from analysis. A p value <
593 0.05 was considered significant. P values are indicated on plots and in figure legends. (* p <
594 0.05, ** p < 0.01, *** p < 0.001).

595 **Supplementary materials**

596 Supplementary Materials and Methods

597 Table S1. Inflammation grading of gut tissue samples from WT and *Igha*$^{-/-}$ mice

598 Table S2. NYC cohort of IGAD patients

599 Table S3. BCN cohort of IGAD patients

600 Fig. S1. IgA enhances systemic IgG3 responses to TI antigens

601 Fig. S2. IgA enhances systemic IgG1 responses to TD antigens without having major effects n T
602 cells ad DCs

603 Fig. S3. IgA restrains systemic IgG and IgM responses to translocated gut antigens

604 Fig. S4. IgA start limiting the gut microbiota-driven expansion of systemic IgG1^{+} B cells and
605 IgG1-secreting plasma cells at an early age

606 Fig. S5. IgA constrains the gut microbiota-driven expansion of PD-1^{+}CD4^{+} T cells in mice and
607 its loss perturbs the frequency of circulating switched memory B cells and plasma cells in
608 humans

609 Fig. S6. IgA optimizes the amount of circulating BCAAs, which show IgG-enhancing potential.

610 **REFERENCES AND NOTES**

611 1. Y. Belkaid, T. W. Hand, Role of the microbiota in immunity and inflammation. *Cell* **157**,
612 121–141 (2014).
613 2. J. L. Sonnenburg, F. Bäckhed, Diet-microbiota interactions as moderators of human
614 metabolism. *Nature* **535**, 56–64 (2016).
615 3. E. Sherwin, S. R. Bordenstein, J. L. Quinn, T. G. Dinan, J. F. Cryan, Microbiota and the
616 social brain. *Science* **366**, eaar2016 (2019).

4. W. E. Ruff, T. M. Greiling, M. A. Kriegel, Host-microbiota interactions in immune-mediated diseases. *Nat Rev Microbiol* **18**, 521–538 (2020).
5. H. Renz, C. Skevaki, Early life microbial exposures and allergy risks: opportunities for prevention. *Nat Rev Immunol* **21**, 177–191 (2021).
6. N. Kamada, S.-U. Seo, G. Y. Chen, G. Núñez, Role of the gut microbiota in immunity and inflammatory disease. *Nat Rev Immunol* **13**, 321–335 (2013).
7. S. E. De Jong, A. Olin, B. Pulendran, The Impact of the Microbiome on Immunity to Vaccination in Humans. *Cell Host & Microbe* **28**, 169–179 (2020).
8. B. B. Finlay, R. Goldszmid, K. Honda, G. Trinchieri, J. Wargo, L. Zitvogel, Can we harness the microbiota to enhance the efficacy of cancer immunotherapy? *Nat Rev Immunol* **20**, 522–528 (2020).
9. V. Gopalakrishnan, C. N. Spencer, L. Nezi, A. Reuben, M. C. Andrews, T. V. Karpinets, P. A. Prieto, D. Vicente, K. Hoffman, S. C. Wei, A. P. Cogdill, L. Zhao, C. W. Hudgens, D. S. Hutchinson, T. Manzo, M. Petaccia de Macedo, T. Cotechini, T. Kumar, W. S. Chen, S. M. Reddy, R. Szczepaniak Sloane, J. Galloway-Pena, H. Jiang, P. L. Chen, E. J. Shpall, K. Rezvani, A. M. Alousi, R. F. Chemaly, S. Shelburne, L. M. Vence, P. C. Okhuysen, V. B. Jensen, A. G. Swennes, F. McAllister, E. Marcelo Riquelme Sanchez, Y. Zhang, E. Le Chatelier, L. Zitvogel, N. Pons, J. L. Austin-Breneman, L. E. Haydu, E. M. Burton, J. M. Gardner, E. Sirmans, J. Hu, A. J. Lazar, T. Tsujikawa, A. Diab, H. Tawbi, I. C. Glitza, W. J. Hwu, S. P. Patel, S. E. Woodman, R. N. Amaria, M. A. Davies, J. E. Gershenwald, P. Hwu, J. E. Lee, J. Zhang, L. M. Coussens, Z. A. Cooper, P. A. Futreal, C. R. Daniel, N. J. Ajami, J. F. Petrosino, M. T. Tetzlaff, P. Sharma, J. P. Allison, R. R. Jenq, J. A. Wargo, Gut microbiome modulates response to anti-PD-1 immunotherapy in melanoma patients. *Science* **359**, 97–103 (2018).
10. K. Chen, G. Magri, E. K. Grasset, A. Cerutti, Rethinking mucosal antibody responses: IgM, IgG and IgD join IgA. *Nat Rev Immunol* **20**, 427–441 (2020).
11. J. J. Bunker, T. M. Flynn, J. C. Koval, D. G. Shaw, M. Meisel, B. D. McDonald, I. E. Ishizuka, A. L. Dent, P. C. Wilson, B. Jabri, D. A. Antonopoulos, A. Bendelac, Innate and Adaptive Humoral Responses Coat Distinct Commensal Bacteria with Immunoglobulin A. *Immunity* **43**, 541–553 (2015).
12. E. K. Grasset, A. Chorny, S. Casas-Recasens, C. Gutzeit, G. Bongers, I. Thomsen, L. Chen, Z. He, D. B. Matthews, M. A. Oropallo, P. Veeramreddy, M. Uzzan, A. Mortha, J. Carrillo, B. S. Reis, M. Ramanujam, J. Sintes, G. Magri, P. J. Maglione, C. Cunningham-Rundles, R. J. Bram, J. Faith, S. Mehandru, O. Pabst, A. Cerutti, Gut T cell-independent IgA responses to commensal bacteria require engagement of the TACI receptor on B cells. *Sci Immunol* **5**, eaat7117 (2020).
13. A. J. Macpherson, B. Yilmaz, J. P. Limenitakis, S. C. Ganal-Vonarburg, IgA Function in Relation to the Intestinal Microbiota. *Annu. Rev. Immunol.* **36**, 359–381 (2018).
14. M. A. Koch, G. L. Reiner, K. A. Lugo, L. S. M. Kreuk, A. G. Stanbery, E. Ansaldo, T. D. Seher, W. B. Ludington, G. M. Barton, Maternal IgG and IgA Antibodies Dampen Mucosal T Helper Cell Responses in Early Life. *Cell* **165**, 827–841 (2016).
15. T. Rollenske, V. Szijarto, J. Lukasiewicz, L. M. Guachalla, K. Stojkovic, K. Hartl, L. Stulik, S. Kocher, F. Lasitschka, M. Al-Saeedi, J. Schröder-Braunstein, M. von Frankenberg, G. Gaebelein, P. Hoffmann, S. Klein, K. Heeg, E. Nagy, G. Nagy, H. Wardemann, Cross-specificity of protective human antibodies against Klebsiella pneumoniae LPS O-antigen. *Nat Immunol* **19**, 617–624 (2018).

16. J. Fadlallah, D. Sterlin, C. Fieschi, C. Parizot, K. Dorgham, H. El Kafsi, G. Autaa, P. Ghillani-Dalbin, C. Juste, P. Lepage, M. Malphettes, L. Galicier, D. Boutboul, K. Clément, S. André, F. Marquet, C. Tresallet, A. Mathian, M. Miyara, E. Oksenhendler, Z. Amoura, H. Yssel, M. Larsen, G. Gorochov, Synergistic convergence of microbiota-specific systemic IgG and secretory IgA. *Journal of Allergy and Clinical Immunology* **143**, 1575-1585.e4 (2019).
17. C. Cunningham-Rundles, P. P. Ponda, Molecular defects in T- and B-cell primary immunodeficiency diseases. *Nat Rev Immunol* **5**, 880–892 (2005).
18. M. Uzzan, H. M. Ko, S. Mehandru, C. Cunningham-Rundles, Gastrointestinal Disorders Associated with Common Variable Immune Deficiency (CVID) and Chronic Granulomatous Disease (CGD). *Curr Gastroenterol Rep* **18**, 17 (2016).
19. J. Fadlallah, H. El Kafsi, D. Sterlin, C. Juste, C. Parizot, K. Dorgham, G. Autaa, D. Gouas, M. Almeida, P. Lepage, N. Pons, E. Le Chatelier, F. Levenez, S. Kennedy, N. Galleron, J.-P. P. De Barros, M. Malphettes, L. Galicier, D. Boutboul, A. Mathian, M. Miyara, E. Oksenhendler, Z. Amoura, J. Doré, C. Fieschi, S. D. Ehrlich, M. Larsen, G. Gorochov, Microbial ecology perturbation in human IgA deficiency. *Sci. Transl. Med.* **10**, eaan1217 (2018).
20. J. R. Catanzaro, J. D. Strauss, A. Bielecka, A. F. Porto, F. M. Lobo, A. Urban, W. B. Schofield, N. W. Palm, IgA-deficient humans exhibit gut microbiota dysbiosis despite secretion of compensatory IgM. *Sci Rep* **9**, 13574 (2019).
21. N. J. Croucher, A. Løchen, S. D. Bentley, Pneumococcal Vaccines: Host Interactions, Population Dynamics, and Design Principles. *Annu Rev Microbiol* **72**, 521–549 (2018).
22. P. J. Lane, I. C. MacLennan, Impaired IgG2 anti-pneumococcal antibody responses in patients with recurrent infection and normal IgG2 levels but no IgA. *Clin Exp Immunol* **65**, 427–433 (1986).
23. E. Edwards, S. Razvi, C. Cunningham-Rundles, IgA deficiency: clinical correlates and responses to pneumococcal vaccine. *Clin Immunol* **111**, 93–97 (2004).
24. A. Aghamohammadi, J. Mohammadi, N. Parvaneh, N. Rezaei, M. Moin, T. Espanol, L. Hammarstrom, Progression of selective IgA deficiency to common variable immunodeficiency. *Int Arch Allergy Immunol* **147**, 87–92 (2008).
25. J. Z. Oh, R. Ravindran, B. Chassaing, F. A. Carvalho, M. S. Maddur, M. Bower, P. Hakimpour, K. P. Gill, H. I. Nakaya, F. Yarovinsky, R. B. Sartor, A. T. Gewirtz, B. Pulendran, TLR5-mediated sensing of gut microbiota is necessary for antibody responses to seasonal influenza vaccination. *Immunity* **41**, 478–492 (2014).
26. T. C. Cullender, B. Chassaing, A. Janzon, K. Kumar, C. E. Muller, J. J. Werner, L. T. Angenent, M. E. Bell, A. G. Hay, D. A. Peterson, J. Walter, M. Vijay-Kumar, A. T. Gewirtz, R. E. Ley, Innate and adaptive immunity interact to quench microbiome flagellar motility in the gut. *Cell Host Microbe* **14**, 571–581 (2013).
27. M. Kim, Y. Qie, J. Park, C. H. Kim, Gut Microbial Metabolites Fuel Host Antibody Responses. *Cell Host Microbe* **20**, 202–214 (2016).
28. Y. Uchimura, T. Fuhrer, H. Li, M. A. Lawson, M. Zimmermann, B. Yilmaz, J. Zindel, F. Ronchi, M. Sorribas, S. Hapfelmeier, S. C. Ganal-Vonarburg, M. Gomez De Agüero, K. D. McCoy, U. Sauer, A. J. Macpherson, Antibodies Set Boundaries Limiting Microbial Metabolite Penetration and the Resultant Mammalian Host Response. *Immunity* **49**, 545-559.e5 (2018).

29. A. Cerutti, M. Cols, I. Puga, Marginal zone B cells: virtues of innate-like antibody-producing lymphocytes. *Nat Rev Immunol* **13**, 118–132 (2013).
30. G. R. Harriman, M. Bogue, P. Rogers, M. Finegold, S. Pacheco, A. Bradley, Y. Zhang, I. N. Mbawuike, Targeted deletion of the IgA constant region in mice leads to IgA deficiency with alterations in expression of other Ig isotypes. *J Immunol* **162**, 2521–2529 (1999).
31. E. J. Pone, J. Zhang, T. Mai, C. A. White, G. Li, J. K. Sakakura, P. J. Patel, A. Al-Qahtani, H. Zan, Z. Xu, P. Casali, BCR-signalling synergizes with TLR-signalling for induction of AID and immunoglobulin class-switching through the non-canonical NF-κB pathway. *Nat Commun* **3**, 767 (2012).
32. S. Crotty, T Follicular Helper Cell Biology: A Decade of Discovery and Diseases. *Immunity* **50**, 1132–1148 (2019).
33. T. Castro-Dopico, T. W. Dennison, J. R. Ferdinand, R. J. Mathews, A. Fleming, D. Clift, B. J. Stewart, C. Jing, K. Strongili, L. I. Labzin, E. J. M. Monk, K. Saeb-Parsy, C. E. Bryant, S. Clare, M. Parkes, M. R. Clatworthy, Anti-commensal IgG Drives Intestinal Inflammation and Type 17 Immunity in Ulcerative Colitis. *Immunity* **50**, 1099-1114.e10 (2019).
34. M. Uzzan, J. C. Martin, L. Mesin, A. E. Livanos, T. Castro-Dopico, R. Huang, F. Petralia, G. Magri, S. Kumar, Q. Zhao, A. K. Rosenstein, M. Tokuyama, K. Sharma, R. Ungaro, R. Kosoy, D. Jha, J. Fischer, H. Singh, M. E. Keir, N. Ramamoorthi, W. E. O'Gorman, B. L. Cohen, A. Rahman, F. Cossarini, A. Seki, L. Leyre, S. T. Vaquero, S. Gurunathan, E. K. Grasset, B. Losic, M. Dubinsky, A. J. Greenstein, Z. Gottlieb, P. Legnani, J. George, H. Irizar, A. Stojmirovic, C. Brodmerkel, A. Kasarkis, B. E. Sands, G. Furtado, S. A. Lira, Z. K. Tuong, H. M. Ko, A. Cerutti, C. O. Elson, M. R. Clatworthy, M. Merad, M. Suárez-Fariñas, C. Argmann, J. A. Hackney, G. D. Victora, G. J. Randolph, E. Kenigsberg, J. F. Colombel, S. Mehandru, Ulcerative colitis is characterized by a plasmablast-skewed humoral response associated with disease activity. *Nat Med* **28**, 766–779 (2022).
35. C. W. Y. Ha, A. Martin, G. D. Sepich-Poore, B. Shi, Y. Wang, K. Gouin, G. Humphrey, K. Sanders, Y. Ratnayake, K. S. L. Chan, G. Hendrick, J. R. Caldera, C. Arias, J. E. Moskowitz, S. J. Ho Sui, S. Yang, D. Underhill, M. J. Brady, S. Knott, K. Kaihara, M. J. Steinbaugh, H. Li, D. P. B. McGovern, R. Knight, P. Fleshner, S. Devkota, Translocation of Viable Gut Microbiota to Mesenteric Adipose Drives Formation of Creeping Fat in Humans. *Cell* **183**, 666-683.e17 (2020).
36. N. W. Palm, M. R. de Zoete, T. W. Cullen, N. A. Barry, J. Stefanowski, L. Hao, P. H. Degnan, J. Hu, I. Peter, W. Zhang, E. Ruggiero, J. H. Cho, A. L. Goodman, R. A. Flavell, Immunoglobulin A coating identifies colitogenic bacteria in inflammatory bowel disease. *Cell* **158**, 1000–1010 (2014).
37. G. Magri, L. Comerma, M. Pybus, J. Sintes, D. Lligé, D. Segura-Garzón, S. Bascones, A. Yeste, E. K. Grasset, C. Gutzeit, M. Uzzan, M. Ramanujam, M. C. van Zelm, R. Albero-González, I. Vazquez, M. Iglesias, S. Serrano, L. Márquez, E. Mercade, S. Mehandru, A. Cerutti, Human Secretory IgM Emerges from Plasma Cells Clonally Related to Gut Memory B Cells and Targets Highly Diverse Commensals. *Immunity* **47**, 118-134.e8 (2017).
38. S. Zhang, Y. Han, W. Schofield, M. Nicosia, P. E. Karell, K. P. Newhall, J. Y. Zhou, R. J. Musich, S. Pan, A. Valujskikh, N. Sangwan, M. Dwidar, Q. Lu, T. S. Stappenbeck, Select symbionts drive high IgA levels in the mouse intestine. *Cell Host Microbe* **31**, 1620-1638.e7 (2023).
39. F.-E. Johansen, M. Pekna, I. N. Norderhaug, B. Haneberg, M. A. Hietala, P. Krajci, C. Betsholtz, P. Brandtzaeg, Absence of Epithelial Immunoglobulin a Transport, with Increased

Mucosal Leakiness, in Polymeric Immunoglobulin Receptor/Secretory Component–Deficient Mice. *The Journal of Experimental Medicine* **190**, 915–922 (1999).
40. W. Shi, Y. Liao, S. N. Willis, N. Taubenheim, M. Inouye, D. M. Tarlinton, G. K. Smyth, P. D. Hodgkin, S. L. Nutt, L. M. Corcoran, Transcriptional profiling of mouse B cell terminal differentiation defines a signature for antibody-secreting plasma cells. *Nat Immunol* **16**, 663–673 (2015).
41. J. D. Planer, Y. Peng, A. L. Kau, L. V. Blanton, I. M. Ndao, P. I. Tarr, B. B. Warner, J. I. Gordon, Development of the gut microbiota and mucosal IgA responses in twins and gnotobiotic mice. *Nature* **534**, 263–266 (2016).
42. M. Gomez de Agüero, S. C. Ganal-Vonarburg, T. Fuhrer, S. Rupp, Y. Uchimura, H. Li, A. Steinert, M. Heikenwalder, S. Hapfelmeier, U. Sauer, K. D. McCoy, A. J. Macpherson, The maternal microbiota drives early postnatal innate immune development. *Science* **351**, 1296–1302 (2016).
43. Z. Sabouri, S. Perotti, E. Spierings, P. Humburg, M. Yabas, H. Bergmann, K. Horikawa, C. Roots, S. Lambe, C. Young, T. D. Andrews, M. Field, A. Enders, J. H. Reed, C. C. Goodnow, IgD attenuates the IgM-induced anergy response in transitional and mature B cells. *Nat Commun* **7**, 13381 (2016).
44. T. Nagaishi, T. Watabe, K. Kotake, T. Kumazawa, T. Aida, K. Tanaka, R. Ono, F. Ishino, T. Usami, T. Miura, S. Hirakata, H. Kawasaki, N. Tsugawa, D. Yamada, K. Hirayama, S. Yoshikawa, H. Karasuyama, R. Okamoto, M. Watanabe, R. S. Blumberg, T. Adachi, Immunoglobulin A-specific deficiency induces spontaneous inflammation specifically in the ileum. *Gut* **71**, 487–496 (2022).
45. T. Okazaki, T. Honjo, PD-1 and PD-1 ligands: from discovery to clinical application. *Int Immunol* **19**, 813–824 (2007).
46. J. C. Cambier, S. B. Gauld, K. T. Merrell, B. J. Vilen, B-cell anergy: from transgenic models to naturally occurring anergic B cells? *Nat Rev Immunol* **7**, 633–643 (2007).
47. J. A. Duty, P. Szodoray, N.-Y. Zheng, K. A. Koelsch, Q. Zhang, M. Swiatkowski, M. Mathias, L. Garman, C. Helms, B. Nakken, K. Smith, A. D. Farris, P. C. Wilson, Functional anergy in a subpopulation of naive B cells from healthy humans that express autoreactive immunoglobulin receptors. *J Exp Med* **206**, 139–151 (2009).
48. I. Isnardi, Y.-S. Ng, L. Menard, G. Meyers, D. Saadoun, I. Srdanovic, J. Samuels, J. Berman, J. H. Buckner, C. Cunningham-Rundles, E. Meffre, Complement receptor 2/CD21- human naive B cells contain mostly autoreactive unresponsive clones. *Blood* **115**, 5026–5036 (2010).
49. J. M. Brenchley, D. C. Douek, Microbial translocation across the GI tract. *Annu Rev Immunol* **30**, 149–173 (2012).
50. H. K. Pedersen, V. Gudmundsdottir, H. B. Nielsen, T. Hyotylainen, T. Nielsen, B. A. H. Jensen, K. Forslund, F. Hildebrand, E. Prifti, G. Falony, E. Le Chatelier, F. Levenez, J. Doré, I. Mattila, D. R. Plichta, P. Pöhö, L. I. Hellgren, M. Arumugam, S. Sunagawa, S. Vieira-Silva, T. Jørgensen, J. B. Holm, K. Trošt, MetaHIT Consortium, K. Kristiansen, S. Brix, J. Raes, J. Wang, T. Hansen, P. Bork, S. Brunak, M. Oresic, S. D. Ehrlich, O. Pedersen, Human gut microbes impact host serum metabolome and insulin sensitivity. *Nature* **535**, 376–381 (2016).
51. L. F. Mager, R. Burkhard, N. Pett, N. C. A. Cooke, K. Brown, H. Ramay, S. Paik, J. Stagg, R. A. Groves, M. Gallo, I. A. Lewis, M. B. Geuking, K. D. McCoy, Microbiome-derived

inosine modulates response to checkpoint inhibitor immunotherapy. *Science* **369**, 1481–1489 (2020).
52. J. Cantor, C. D. Browne, R. Ruppert, C. C. Féral, R. Fässler, R. C. Rickert, M. H. Ginsberg, CD98hc facilitates B cell proliferation and adaptive humoral immunity. *Nat Immunol* **10**, 412–419 (2009).
53. H. Zhang, G. Alsaleh, J. Feltham, Y. Sun, G. Napolitano, T. Riffelmacher, P. Charles, L. Frau, P. Hublitz, Z. Yu, S. Mohammed, A. Ballabio, S. Balabanov, J. Mellor, A. K. Simon, Polyamines Control eIF5A Hypusination, TFEB Translation, and Autophagy to Reverse B Cell Senescence. *Mol Cell* **76**, 110-125.e9 (2019).
54. E. Ansaldo, L. C. Slayden, K. L. Ching, M. A. Koch, N. K. Wolf, D. R. Plichta, E. M. Brown, D. B. Graham, R. J. Xavier, J. J. Moon, G. M. Barton, Akkermansia muciniphila induces intestinal adaptive immune responses during homeostasis. *Science* **364**, 1179–1184 (2019).
55. M. Y. Zeng, D. Cisalpino, S. Varadarajan, J. Hellman, H. S. Warren, M. Cascalho, N. Inohara, G. Núñez, Gut Microbiota-Induced Immunoglobulin G Controls Systemic Infection by Symbiotic Bacteria and Pathogens. *Immunity* **44**, 647–658 (2016).
56. T. Hagan, M. Cortese, N. Rouphael, C. Boudreau, C. Linde, M. S. Maddur, J. Das, H. Wang, J. Guthmiller, N.-Y. Zheng, M. Huang, A. A. Uphadhyay, L. Gardinassi, C. Petitdemange, M. P. McCullough, S. J. Johnson, K. Gill, B. Cervasi, J. Zou, A. Bretin, M. Hahn, A. T. Gewirtz, S. E. Bosinger, P. C. Wilson, S. Li, G. Alter, S. Khurana, H. Golding, B. Pulendran, Antibiotics-Driven Gut Microbiome Perturbation Alters Immunity to Vaccines in Humans. *Cell* **178**, 1313-1328.e13 (2019).
57. S. Kawamoto, T. H. Tran, M. Maruya, K. Suzuki, Y. Doi, Y. Tsutsui, L. M. Kato, S. Fagarasan, The inhibitory receptor PD-1 regulates IgA selection and bacterial composition in the gut. *Science* **336**, 485–489 (2012).
58. A. Nakajima, A. Vogelzang, M. Maruya, M. Miyajima, M. Murata, A. Son, T. Kuwahara, T. Tsuruyama, S. Yamada, M. Matsuura, H. Nakase, D. A. Peterson, S. Fagarasan, K. Suzuki, IgA regulates the composition and metabolic function of gut microbiota by promoting symbiosis between bacteria. *J Exp Med* **215**, 2019–2034 (2018).
59. J. Mirpuri, M. Raetz, C. R. Sturge, C. L. Wilhelm, A. Benson, R. C. Savani, L. V. Hooper, F. Yarovinsky, Proteobacteria-specific IgA regulates maturation of the intestinal microbiota. *Gut Microbes* **5**, 28–39 (2014).
60. T. Rollenske, S. Burkhalter, L. Muerner, S. von Gunten, J. Lukasiewicz, H. Wardemann, A. J. Macpherson, Parallelism of intestinal secretory IgA shapes functional microbial fitness. *Nature* **598**, 657–661 (2021).
61. E. L. Kuan, S. Ivanov, E. A. Bridenbaugh, G. Victora, W. Wang, E. W. Childs, A. M. Platt, C. V. Jakubzick, R. J. Mason, A. A. Gashev, M. Nussenzweig, M. A. Swartz, M. L. Dustin, D. C. Zawieja, G. J. Randolph, Collecting lymphatic vessel permeability facilitates adipose tissue inflammation and distribution of antigen to lymph node-homing adipose tissue dendritic cells. *J Immunol* **194**, 5200–5210 (2015).
62. L. H. Jackson-Jones, P. Smith, J. R. Portman, M. S. Magalhaes, K. J. Mylonas, M. M. Vermeren, M. Nixon, B. E. P. Henderson, R. Dobie, S. Vermeren, L. Denby, N. C. Henderson, D. J. Mole, C. Bénézech, Stromal Cells Covering Omental Fat-Associated Lymphoid Clusters Trigger Formation of Neutrophil Aggregates to Capture Peritoneal Contaminants. *Immunity* **52**, 700-715.e6 (2020).

63. I. Wernstedt Asterholm, C. Tao, T. S. Morley, Q. A. Wang, F. Delgado-Lopez, Z. V. Wang, P. E. Scherer, Adipocyte inflammation is essential for healthy adipose tissue expansion and remodeling. *Cell Metab* **20**, 103–118 (2014).
64. C. Bénézech, N.-T. Luu, J. A. Walker, A. A. Kruglov, Y. Loo, K. Nakamura, Y. Zhang, S. Nayar, L. H. Jones, A. Flores-Langarica, A. McIntosh, J. Marshall, F. Barone, G. Besra, K. Miles, J. E. Allen, M. Gray, G. Kollias, A. F. Cunningham, D. R. Withers, K. M. Toellner, N. D. Jones, M. Veldhoen, S. A. Nedospasov, A. N. J. McKenzie, J. H. Caamaño, Inflammation-induced formation of fat-associated lymphoid clusters. *Nat Immunol* **16**, 819–828 (2015).
65. C. Perez-Shibayama, C. Gil-Cruz, H.-W. Cheng, L. Onder, A. Printz, U. Mörbe, M. Novkovic, C. Li, C. Lopez-Macias, M. B. Buechler, S. J. Turley, M. Mack, C. Soneson, M. D. Robinson, E. Scandella, J. Gommerman, B. Ludewig, Fibroblastic reticular cells initiate immune responses in visceral adipose tissues and secure peritoneal immunity. *Sci Immunol* **3**, eaar4539 (2018).
66. G. P. Donaldson, M. S. Ladinsky, K. B. Yu, J. G. Sanders, B. B. Yoo, W.-C. Chou, M. E. Conner, A. M. Earl, R. Knight, P. J. Bjorkman, S. K. Mazmanian, Gut microbiota utilize immunoglobulin A for mucosal colonization. *Science* **360**, 795–800 (2018).
67. J. J. Faith, P. P. Ahern, V. K. Ridaura, J. Cheng, J. I. Gordon, Identifying gut microbe-host phenotype relationships using combinatorial communities in gnotobiotic mice. *Sci Transl Med* **6**, 220ra11 (2014).
68. D. E. Briles, J. Latham Claflin, K. Schroer, C. Forman, Mouse IgG3 antibodies are highly protective against infection with Streptococcus pneumoniae. *Nature* **294**, 88–90 (1981).
69. G. R. Siber, P. H. Schur, A. C. Aisenberg, S. A. Weitzman, G. Schiffman, Correlation between Serum IgG-2 Concentrations and the Antibody Response to Bacterial Polysaccharide Antigens. *New England Journal of Medicine* **303**, 178–182 (1980).
70. A. Aghamohammadi, T. Cheraghi, M. Gharagozlou, M. Movahedi, N. Rezaei, M. Yeganeh, N. Parvaneh, H. Abolhassani, Z. Pourpak, M. Moin, IgA deficiency: correlation between clinical and immunological phenotypes. *J Clin Immunol* **29**, 130–136 (2009).
71. H. Sokol, C. Lay, P. Seksik, G. W. Tannock, Analysis of bacterial bowel communities of IBD patients: what has it revealed? *Inflamm Bowel Dis* **14**, 858–867 (2008).
72. A. Chudnovskiy, A. Mortha, V. Kana, A. Kennard, J. D. Ramirez, A. Rahman, R. Remark, I. Mogno, R. Ng, S. Gnjatic, E.-A. D. Amir, A. Solovyov, B. Greenbaum, J. Clemente, J. Faith, Y. Belkaid, M. E. Grigg, M. Merad, Host-Protozoan Interactions Protect from Mucosal Infections through Activation of the Inflammasome. *Cell* **167**, 444-456.e14 (2016).
73. M. R. Hepworth, L. A. Monticelli, T. C. Fung, C. G. K. Ziegler, S. Grunberg, R. Sinha, A. R. Mantegazza, H.-L. Ma, A. Crawford, J. M. Angelosanto, E. J. Wherry, P. A. Koni, F. D. Bushman, C. O. Elson, G. Eberl, D. Artis, G. F. Sonnenberg, Innate lymphoid cells regulate CD4+ T-cell responses to intestinal commensal bacteria. *Nature* **498**, 113–117 (2013).
74. M. D. Robinson, A. Oshlack, A scaling normalization method for differential expression analysis of RNA-seq data. *Genome Biol* **11**, R25 (2010).
75. I. Wanigasuriya, Q. Gouil, S. A. Kinkel, A. Tapia del Fierro, T. Beck, E. A. Roper, K. Breslin, J. Stringer, K. Hutt, H. J. Lee, A. Keniry, M. E. Ritchie, M. E. Blewitt, Smchd1 is a maternal effect gene required for genomic imprinting. *eLife* **9**, e55529 (2020).
76. C. W. Law, Y. Chen, W. Shi, G. K. Smyth, voom: Precision weights unlock linear model analysis tools for RNA-seq read counts. *Genome Biol* **15**, R29 (2014).
77. R. M. Smith, Detecting item bias with the Rasch model. *J Appl Meas* **5**, 430–449 (2004).

78. S. Durinck, Y. Moreau, A. Kasprzyk, S. Davis, B. De Moor, A. Brazma, W. Huber, BioMart and Bioconductor: a powerful link between biological databases and microarray data analysis. *Bioinformatics* **21**, 3439–3440 (2005).
79. S. Durinck, P. T. Spellman, E. Birney, W. Huber, Mapping identifiers for the integration of genomic datasets with the R/Bioconductor package biomaRt. *Nat Protoc* **4**, 1184–1191 (2009).
80. S. Hänzelmann, R. Castelo, J. Guinney, GSVA: gene set variation analysis for microarray and RNA-seq data. *BMC Bioinformatics* **14**, 7 (2013).
81. L. R. Thompson, J. G. Sanders, D. McDonald, A. Amir, J. Ladau, K. J. Locey, R. J. Prill, A. Tripathi, S. M. Gibbons, G. Ackermann, J. A. Navas-Molina, S. Janssen, E. Kopylova, Y. Vázquez-Baeza, A. González, J. T. Morton, S. Mirarab, Z. Zech Xu, L. Jiang, M. F. Haroon, J. Kanbar, Q. Zhu, S. Jin Song, T. Kosciolek, N. A. Bokulich, J. Lefler, C. J. Brislawn, G. Humphrey, S. M. Owens, J. Hampton-Marcell, D. Berg-Lyons, V. McKenzie, N. Fierer, J. A. Fuhrman, A. Clauset, R. L. Stevens, A. Shade, K. S. Pollard, K. D. Goodwin, J. K. Jansson, J. A. Gilbert, R. Knight, Earth Microbiome Project Consortium, A communal catalogue reveals Earth's multiscale microbial diversity. *Nature* **551**, 457–463 (2017).
82. E. Bolyen, J. R. Rideout, M. R. Dillon, N. A. Bokulich, C. C. Abnet, G. A. Al-Ghalith, H. Alexander, E. J. Alm, M. Arumugam, F. Asnicar, Y. Bai, J. E. Bisanz, K. Bittinger, A. Brejnrod, C. J. Brislawn, C. T. Brown, B. J. Callahan, A. M. Caraballo-Rodríguez, J. Chase, E. K. Cope, R. Da Silva, C. Diener, P. C. Dorrestein, G. M. Douglas, D. M. Durall, C. Duvallet, C. F. Edwardson, M. Ernst, M. Estaki, J. Fouquier, J. M. Gauglitz, S. M. Gibbons, D. L. Gibson, A. Gonzalez, K. Gorlick, J. Guo, B. Hillmann, S. Holmes, H. Holste, C. Huttenhower, G. A. Huttley, S. Janssen, A. K. Jarmusch, L. Jiang, B. D. Kaehler, K. B. Kang, C. R. Keefe, P. Keim, S. T. Kelley, D. Knights, I. Koester, T. Kosciolek, J. Kreps, M. G. I. Langille, J. Lee, R. Ley, Y.-X. Liu, E. Loftfield, C. Lozupone, M. Maher, C. Marotz, B. D. Martin, D. McDonald, L. J. McIver, A. V. Melnik, J. L. Metcalf, S. C. Morgan, J. T. Morton, A. T. Naimey, J. A. Navas-Molina, L. F. Nothias, S. B. Orchanian, T. Pearson, S. L. Peoples, D. Petras, M. L. Preuss, E. Pruesse, L. B. Rasmussen, A. Rivers, M. S. Robeson, P. Rosenthal, N. Segata, M. Shaffer, A. Shiffer, R. Sinha, S. J. Song, J. R. Spear, A. D. Swafford, L. R. Thompson, P. J. Torres, P. Trinh, A. Tripathi, P. J. Turnbaugh, S. Ul-Hasan, J. J. J. van der Hooft, F. Vargas, Y. Vázquez-Baeza, E. Vogtmann, M. von Hippel, W. Walters, Y. Wan, M. Wang, J. Warren, K. C. Weber, C. H. D. Williamson, A. D. Willis, Z. Z. Xu, J. R. Zaneveld, Y. Zhang, Q. Zhu, R. Knight, J. G. Caporaso, Reproducible, interactive, scalable and extensible microbiome data science using QIIME 2. *Nat Biotechnol* **37**, 852–857 (2019).
83. B. J. Callahan, P. J. McMurdie, M. J. Rosen, A. W. Han, A. J. A. Johnson, S. P. Holmes, DADA2: High-resolution sample inference from Illumina amplicon data. *Nat Methods* **13**, 581–583 (2016).
84. D. McDonald, M. N. Price, J. Goodrich, E. P. Nawrocki, T. Z. DeSantis, A. Probst, G. L. Andersen, R. Knight, P. Hugenholtz, An improved Greengenes taxonomy with explicit ranks for ecological and evolutionary analyses of bacteria and archaea. *ISME J* **6**, 610–618 (2012).
85. G. M. Douglas, V. J. Maffei, J. R. Zaneveld, S. N. Yurgel, J. R. Brown, C. M. Taylor, C. Huttenhower, M. G. I. Langille, PICRUSt2 for prediction of metagenome functions. *Nat Biotechnol* **38**, 685–688 (2020).
86. C. Lozupone, R. Knight, UniFrac: a new phylogenetic method for comparing microbial communities. *Appl Environ Microbiol* **71**, 8228–8235 (2005).

936 87. N. Segata, J. Izard, L. Waldron, D. Gevers, L. Miropolsky, W. S. Garrett, C. Huttenhower,
937 Metagenomic biomarker discovery and explanation. *Genome Biol* **12**, R60 (2011).
938 88. S. Mandal, W. Van Treuren, R. A. White, M. Eggesbø, R. Knight, S. D. Peddada, Analysis
939 of composition of microbiomes: a novel method for studying microbial composition. *Microb*
940 *Ecol Health Dis* **26**, 27663 (2015).
941

942 **Acknowledgments**

943 **Funding:** Supported by US National Institutes of Health grant P01 AI61093 to C. Cunningham-
944 Rundels and A. Cerutti, R01 DK123749 to A. Cerutti, J. .J. Faith. and S. Mehandru, R01
945 DK114038 to J. Clemente and K23 AI137183 to P. J. Maglione; Ministerio de Ciencia,
946 Innovación y Universidades grant RTI2018-093894-B-I00 and European Advanced Grant ERC-
947 2011-ADG-20110310 to A. Cerutti, and the Institute of Health Carlos III-Miguel Servet research
948 program to G. Magri.

949 **Author Contributions:**

950 Conceptualization: AC, CG, EKG

951 Methodology: CG, EKG, PJM, GM, GJB, AMN, MGP, MMG, RDC, MS-F, JCC, M.S-F, JJF,
952 CC-R, AC

953 Investigation: CG, EKG, DBM, GJB, HM, GM, LT, MP, STV, LR, RT-P, MP, PKV, AMN,
954 MGP, MMG, RDC

955 Visualization: CG, EKG, DBM, GM, GJB, LT

956 Funding acquisition: AC, CCR, JJF, SM, GM, PJM

957 Project administration: AC, CG

958 Supervision: AC, CG, EKG

959 Writing – original draft: AC, EKG

960 Writing – review & editing: AC, EKG, JJF, JCC, CG, CC-R, DBM, MG, AMN, MGP, MMG,
961 RDC, SM

962 **Competing Interests:** The authors declare that they have no competing financial interests.

Data and materials availability: The authors declare that all data supporting the findings of this study are available within the article and its supplementary information files or from the corresponding authors upon request. RNA-seq sequence data files (fastq) are stored in the public sequence read archive (SRA) under project number GSE173361 (reviewer token: abizcussbtwtzgh); 16S sequence data files (fastq) are stored in the public SRA under project number PRJNA722766 (reviewer link: https://dataview.ncbi.nlm.nih.gov/object/PRJNA722766?reviewer=4nf2agqsarp8ni0iaei1flufa).

970 **FIGURES**

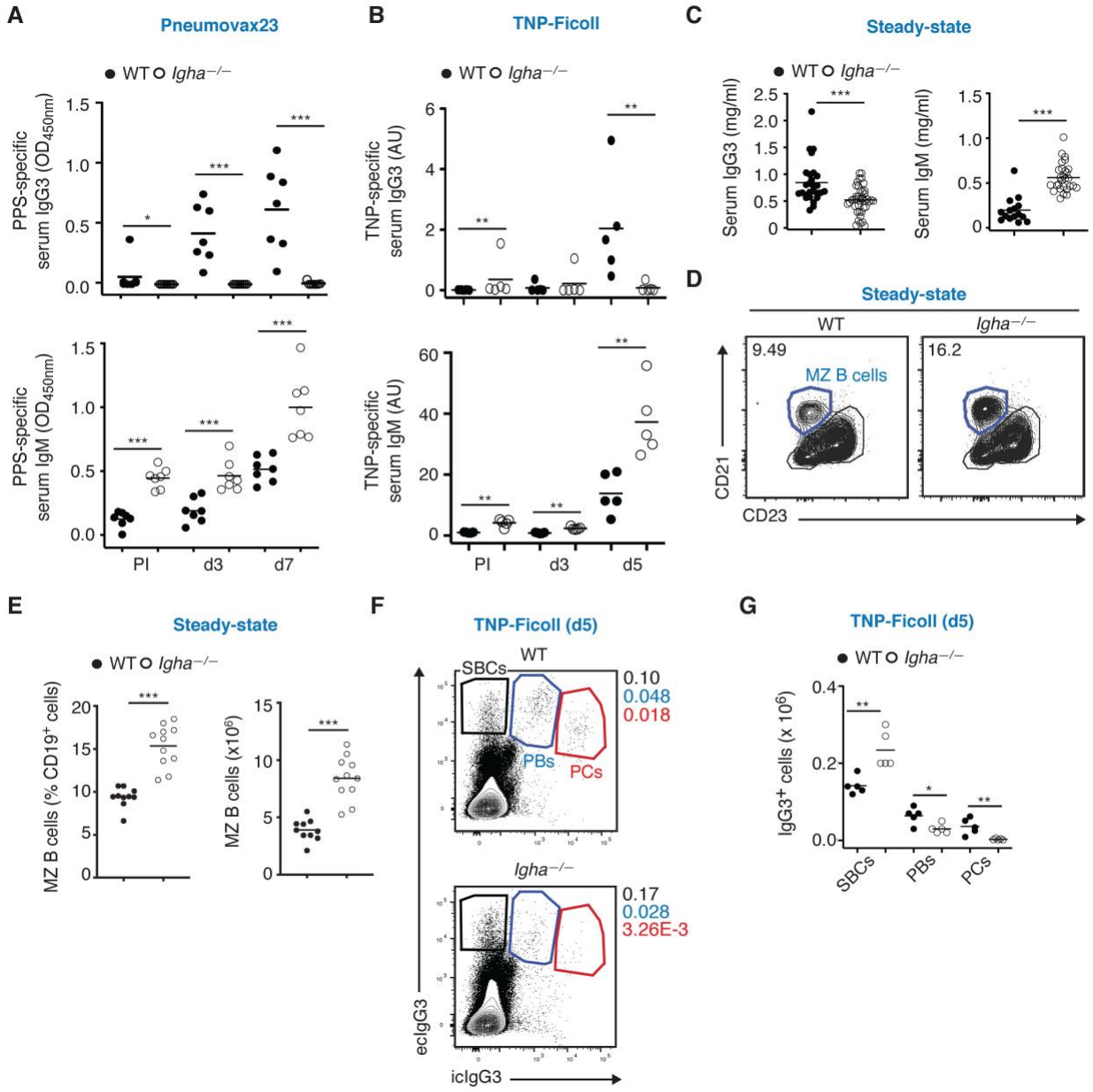

971

972 **Fig. 1. IgA enhances systemic IgG responses to TI immunizations**. (**A**) ELISA of serum IgG3
973 (top) and IgM (bottom) to PPS in 7 WT or *Igha*$^{-/-}$ mice prior to immunization (PI) and 3 or 7
974 days following Pneumovax23 i.v. immunization. (**B**) ELISA of serum IgG3 (top) and IgM
975 (bottom) to TNP from 5 WT or *Igha*$^{-/-}$ mice before and 3 or 5 days following i.v. TNP-Ficoll
976 immunization. WT mice in this experiment from JAX. (**C**) ELISA of total serum IgG3 and IgM

977 in 15-27 WT or 28-41 *Igha*$^{-/-}$ mice at steady state. (**D**) Flow cytometry of CD21^{hi}CD23^{lo} splenic
978 MZ B cells from representative WT or *Igha*$^{-/-}$ mice. Numbers indicate MZ B cell frequency of
979 CD19^{+} cells. (**E**) Frequency (% of CD19^{+} cells; left) and absolute number (right) of splenic MZ
980 B cells from 10 WT or 11 *Igha*$^{-/-}$ mice. (**F-G**) Flow cytometry of intracellular (ic) IgG3 and
981 extracellular (ec) IgG3 from splenic ecIgG3^{+}icIgG3^{-} switched B cells (SBCs), ecIgG3^{+}icIgG3^{+}
982 plasmablasts (PBs) and ecIgG3^{lo}icIgG3^{+} PCs of representative WT or *Igha*$^{-/-}$ mice (F) as well as
983 absolute number (G) of SBCs, PBs and PCs from 5 WT or 5 *Igha*$^{-/-}$ mice 5 days following TNP-
984 Ficoll i.v. immunization. Numbers (F) indicate frequency within total cells (F). WT mice in this
985 experiment from JAX. Data show representative flow plots (D, F) or summarize results from one
986 (A, B, E, G) or 5-6 experiments (C). Results are shown with mean; two-tailed unpaired Student's
987 t-test was performed when data followed a Gaussian distribution, otherwise Mann-Whitney test
988 was used. *$p < 0.05$, **$p < 0.01$, ***$p < 0.001$.
989

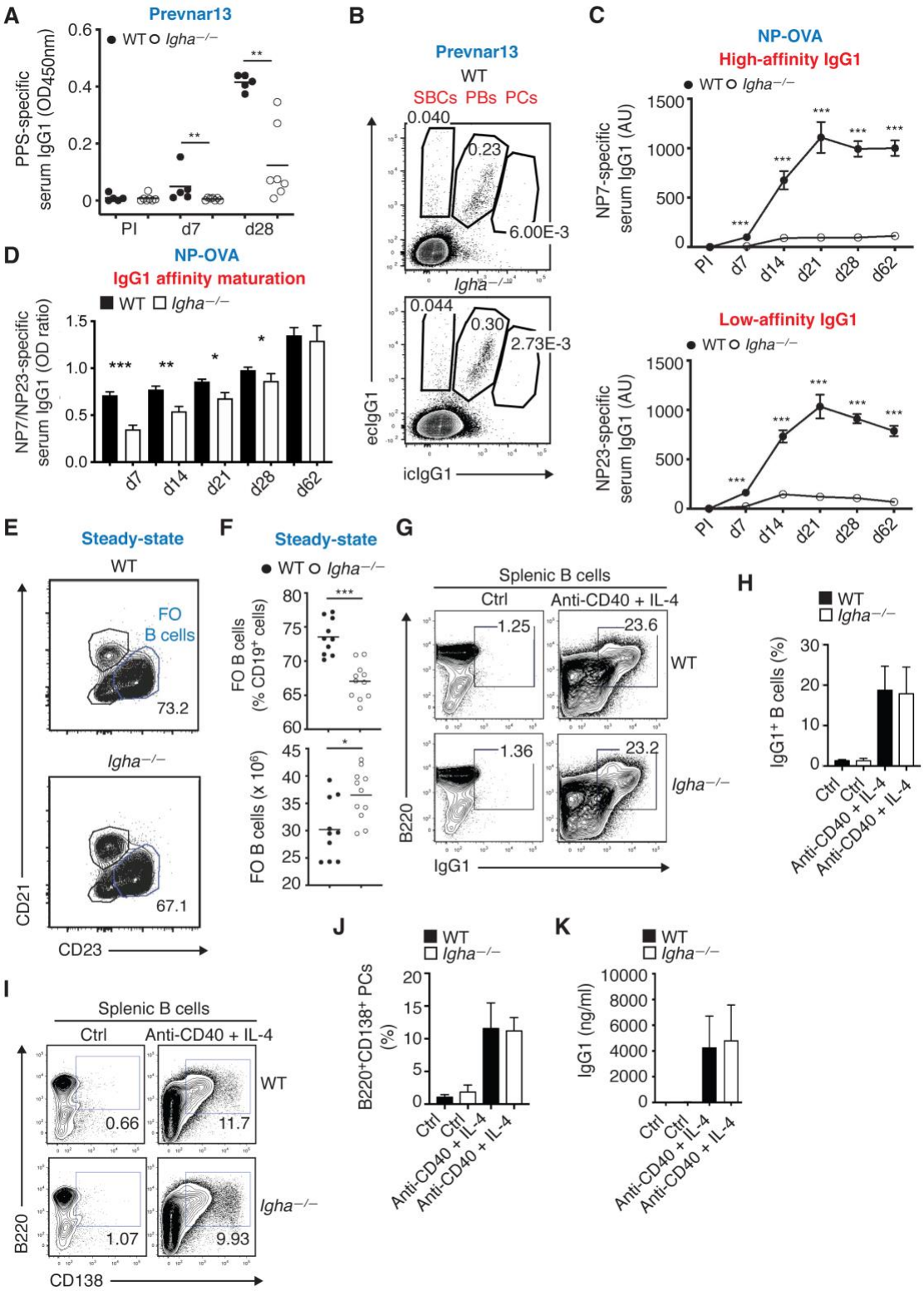

990

991 **Fig. 2. IgA increases systemic IgG responses to TD immunizations**. (**A**) ELISA of serum

992 IgG1 to PPS from 5 WT or 7 *Igha*$^{-/-}$ mice prior to immunization (PI) and 7 or 28 days following

i.v. immunization with Prevnar13. (**B**) Flow cytometry of intracellular (ic) IgG1 and extracellular (ec) IgG1 from splenic ecIgG1^{+}icIgG1^{-} switched B cells (SBCs), ecIgG1^{+}icIgG1^{+} plasmablasts (PBs) and ecIgG1^{lo}icIgG1^{+} PCs of representative WT or *Igha*$^{-/-}$ mice 28 days following i.v. immunization with Prevnar13. Numbers indicate frequency (% of B220^{+} cells) of SBCs, PBs and PCs. (**C**) ELISA of serum high-affinity (NP7-BSA) IgG1 and low-affinity (NP23-BSA) IgG1 from 13 WT or 11 *Igha*$^{-/-}$ mice before immunization (PI) and 7, 14, 21, 28 or 62 days following i.p. immunization with NP15-OVA and alum. (**D**) Affinity maturation of IgG1 calculated as an OD value ratio of IgG1 specific to NP7-BSA versus IgG1 specific to NP23-BSA in 13 WT or 11 *Igha*$^{-/-}$ mice 7, 14, 21, 28 or 62 days following i.p. immunization with NP15-OVA and alum. (**E-F**) Flow cytometry of CD21 and CD23 on splenic FO B cells from representative WT or *Igha*$^{-/-}$ mice at steady state (E) as well as frequency (% of CD19+ cells) and absolute number of CD21^{low}CD23^{high} FO B cells from 10 WT or 11 *Igha*$^{-/-}$ mice (F). (**G, H**) Flow cytometry of B220 and IgG1 on purified splenic B cells from representative WT or *Igha*$^{-/-}$ mice incubated with medium alone (ctrl) or anti-CD40 and IL-4 for 6 days (G) as well as frequency (% of live cells) of splenic IgG1^{+}B220^{+} B cells from 6 WT or *Igha*$^{-/-}$ mice cultured as above (H). (**I-J**) Flow cytometry of B220 and CD138 on purified splenic B cells from representative WT or *Igha*$^{-/-}$ mice incubated with medium alone (ctrl) or anti-CD40 and IL-4 for 6 days (I) as well as frequency (% of live cells) of splenic B220^{+}CD138^{+} PBs from 6 WT or *Igha*$^{-/-}$ mice cultured as above (J). (**K**) ELISA of IgG1 secreted by purified splenic B cells from representative 4 WT or *Igha*$^{-/-}$ mice incubated with medium alone (ctrl) or anti-CD40 and IL-4 for 6 days. Data show one representative result (B, E, G, I) or summarize results from either a single (F), two (A, C, D, K), or three experiments (H, J) Results are shown with mean (A, F) or mean ± s.e.m. (C, D, H, J, K); a two-tailed unpaired Student's t-test was performed when data followed a Gaussian

1016 distribution, otherwise a Mann-Whitney test was used to determine significance. *p < 0.05, **p

1017 < 0.01, ***p <0.001.

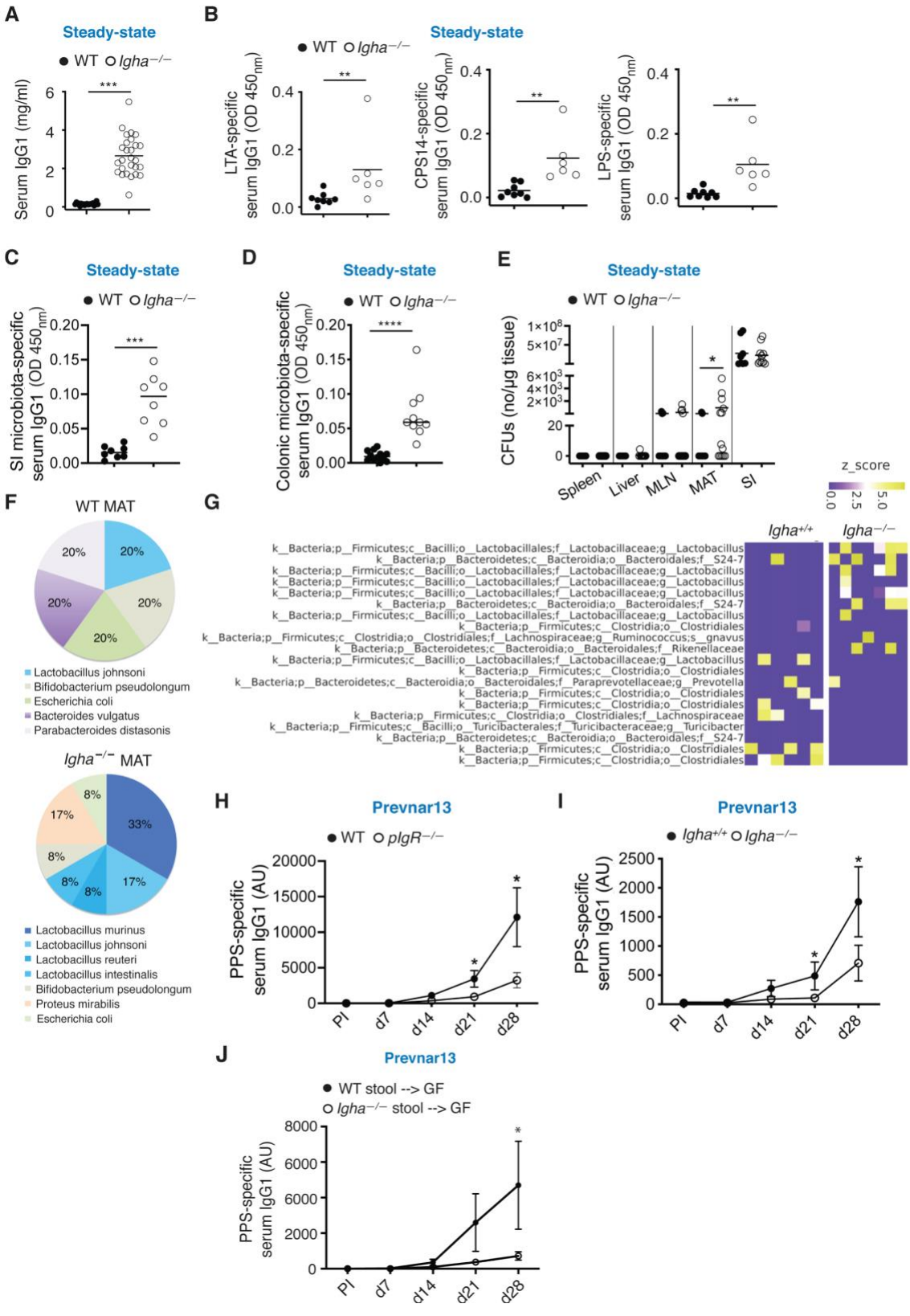
A
Steady-state
WT Igha−/−
Serum IgG1 (mg/ml)
B
Steady-state
WT Igha−/−
LTA-specific serum IgG1 (OD 450nm)
CPS14-specific serum IgG1 (OD 450nm)
LPS-specific serum IgG1 (OD 450nm)
C
Steady-state
SI microbiota-specific serum IgG1 (OD 450nm)
D
Steady-state
Colonic microbiota-specific serum IgG1 (OD 450nm)
E
Steady-state
CFUs (no/µg tissue)
Spleen
Liver
MLN
MAT
SI
F
WT MAT
Lactobacillus johnsoni
Bifidobacterium pseudolongum
Escherichia coli
Bacteroides vulgatus
Parabacteroides distasonis
Igha−/− MAT
Lactobacillus murinus
Lactobacillus johnsoni
Lactobacillus reuteri
Lactobacillus intestinalis
Bifidobacterium pseudolongum
Proteus mirabilis
Escherichia coli
G
z_score
Igha+/+
Igha−/−
k__Bacteria;p__Firmicutes;c__Bacilli;o__Lactobacillales;f__Lactobacillaceae;g__Lactobacillus
k__Bacteria;p__Bacteroidetes;c__Bacteroidia;o__Bacteroidales;f__S24-7
k__Bacteria;p__Firmicutes;c__Clostridia;o__Clostridiales
k__Bacteria;p__Firmicutes;c__Clostridia;o__Ruminococcus;s__gnavus
k__Bacteria;p__Bacteroidetes;c__Bacteroidia;o__Bacteroidales;f__Rikenellaceae
k__Bacteria;p__Bacteroidetes;c__Bacteroidia;o__Bacteroidales;f__Prevotellaceae;g__Prevotella
k__Bacteria;p__Firmicutes;c__Clostridia;o__Clostridiales;f__Lachnospiraceae
k__Bacteria;p__Firmicutes;c__Bacilli;o__Turicibacterales;f__Turicibacteraceae;g__Turicibacter
H
Prevnar13
WT PIgR−/−
PPS-specific serum IgG1 (AU)
PI
d7
d14
d21
d28
I
Prevnar13
Igha+/+ Igha−/−
PPS-specific serum IgG1 (AU)
J
Prevnar13
WT stool --> GF
Igha−/− stool --> GF
PPS-specific serum IgG1 (AU)

1018

Fig. 3. IgA enhances vaccine-specific IgG responses while restraining IgG responses to translocated gut antigens. (**A**) ELISA of total serum IgG1 from 20 WT or 27 *Igha*$^{-/-}$ mice at steady state. (**B**) ELISA of serum IgG1 to lipoteichoic acid (LTA) from *Staphylococcus aureus*, CPS14 from *Streptococcus pneumoniae* or LPS from *Salmonella typhimurium* in 8 WT or 6 *Igha*$^{-/-}$ littermate mice at steady state. (**C, D**) ELISA of serum IgG1 to bacteria inhabiting paired small intestine (SI) (C) or colon (D) fecal samples obtained from 8-12 WT or 8-10 *Igha*$^{-/-}$ mice (fecal and serum samples from same mouse). The microbiota was processed through a freeze-thaw protocol. (**E**) Quantification of CFUs of anaerobic bacteria in homogenates of spleen, liver, MLNs, MAT and SI from 8-13 WT or 9-13 *Igha*$^{-/-}$ mice. (**F**) Taxonomic classification of anaerobic bacterial colonies isolated in the MAT from 2 WT or 7 *Igha*$^{-/-}$ mice, as determined by mass spectrometry. (**G**) 16S rDNA gene sequencing analysis of microbiota from colon feces of 6 WT or 7 *Igha*$^{-/-}$ co-housed littermate mice. (**H**) ELISA of serum IgG1 to PPS from 9 WT mice or 10 *Pigr*$^{-/-}$ mice prior to immunization (PI) and 7, 14, 21 or 28 days following i.p. immunization with Prevnar13. (**I**) ELISA of serum IgG1 to PPS from 11 *Igha*$^{+/+}$ or 16 *Igha*$^{-/-}$ co-housed littermate mice from *Igha*+/- parents prior to immunization (PI) and 7, 14, 21, or 28 days following i.p. immunization with Prevnar13. (**J**) ELISA of serum IgG1 to PPS PI or 7, 14, 21 or 28 days following i.p. immunization with Prevnar13 of ex-GF mice obtained by reconstituting 6-7 GF recipient mice with cecal content from either an SPF WT or an SPF *Igha*$^{-/-}$ donor mouse. Recipient mice were vaccinated two weeks following reconstitution. Measurements were performed four weeks following reconstitution of the gut microbiota. Results summarize 5 (A, E, F), 1 (B, G, J) or 2 (C, D, H, I) independent experiments. Data are presented as mean ± s.e.m.; a two-tailed unpaired Student's t-test was performed when data followed a Gaussian distribution, otherwise a Mann-Whitney test was used. *$p < 0.05$, **$p < 0.01$, ***$p < 0.001$, ****$p < 0.0001$.

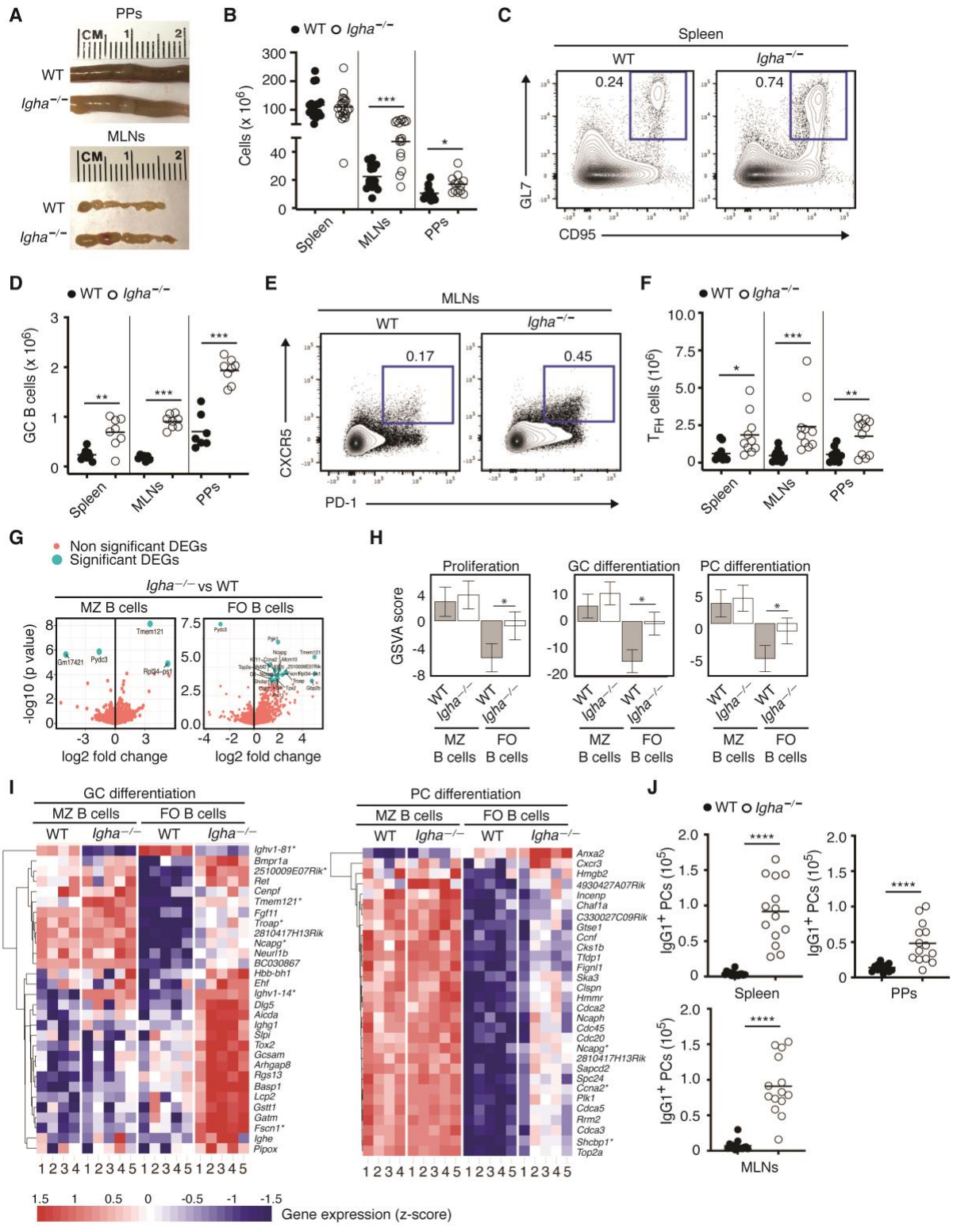

Fig. 4. IgA restrains expansion of IgG1$^+$ GC B cells and IgG1$^+$ PC differentiation. (**A**) Images of PPs and MLNs from representative WT or *Igha*$^{-/-}$ mice. (**B**) Number of total cells in

spleen, MLNs and PPs from 11-19 WT or 12-20 *Igha*$^{-/-}$ mice. (**C-D**) Flow cytometry analysis of splenic CD95^{+}GL7^{+} GC B cells from representative WT or *Igha*$^{-/-}$ mice (C) and absolute number of these cells in spleen, MLNs and PPs from 7-8 WT or 8 *Igha*$^{-/-}$ mice. GC B cells were analyzed from an initial CD45^{+}B220^{+} gate. (**E-F**) PD-1^{+}CXCR5^{+} T_{FH} cells from MLNs of representative WT or *Igha*$^{-/-}$ mice (E) and absolute number of these T_{FH} cells in spleen, MLNs and Peyer's patches from 10-11 WT or 11 *Igha*$^{-/-}$ mice (F). T_{FH} cells were analyzed from an initial CD45^{+}CD19^{-}TCRβ^{+}CD4^{+} gate. (**G**) Volcano plot visualization of differentially expressed genes (DEGs) identified by RNA-seq in splenic MZ and FO B cell from 4-5 WT or 5 *Igha*$^{-/-}$ mice. (**H**) Gene set variation analysis (GSVA) of proliferation (G2-M checkpoint), GC differentiation and PC differentiation gene signatures identified by RNA-seq and differentially expressed by splenic FO but not MZ B cells from 4 WT or 5 *Igha*$^{-/-}$ mice. (**I**) Heat map visualization of z-score for top 30 DEGs related to GC differentiation (left) and PC differentiation (right) gene sets identified by RNA-seq in splenic FO but not MZ B cells from 4-5 WT or 5 *Igha*$^{-/-}$ mice (as in H). Asterisks indicate highly differentially expressed genes discussed in the text. The scale bar shows color coding (blue, white, red) for z-score. (**J**) Absolute numbers of IgG1^{+} PCs in spleen, MLNs and PPs from 14 WT or *Igha*$^{-/-}$ mice. PCs were analyzed from an initial IgD^{lo}CD45^{+} gate (as in Fig. S4B). Data show representative images or flow plots (A, C, E), summarize 2 (J), 3 (D), 6 (B) or one (G-I) independent experiments or summarize 3 experiments representative of 5 (F). Data are presented with mean (B, D, F), median (J), or mean GSVA score and 95% confidence interval (H); a two-tailed unpaired Student's t-test was performed when data were determined to follow a Gaussian distribution (B), otherwise a Mann-Whitney test was used (D, F, J), or limma modeling (H). *$p < 0.05$, **$p < 0.01$, ***$p < 0.001$.

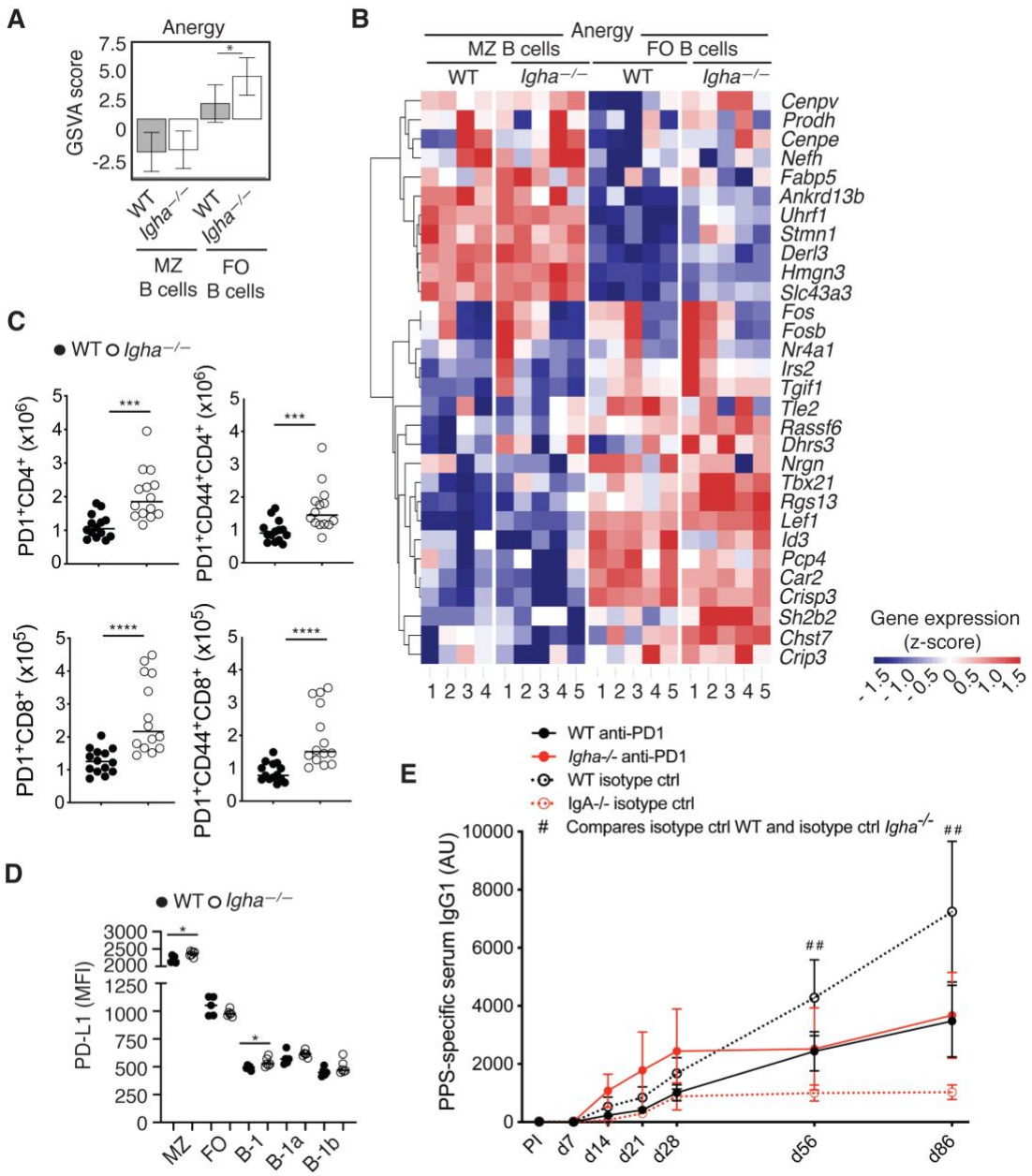

Fig. 5. IgA constrains activation-induced T cell expression of the immune inhibitor PD-1 and anti-PD-1 improves vaccine-specific IgG production in IgA deficiency. (**A**) Gene set variation analysis (GSVA) of anergy gene signatures identified by RNA-seq and differentially expressed by splenic MZ and FO B cells from 4-5 WT or 5 *Igha*$^{-/-}$ mice at steady state. (**B**) Heat map shows z-score of gene-expression for top 30 differentially expressed anergy genes identified

by RNA-seq from gene set differentially expressed (in B) by splenic FO but not MZ B cells from 4-5 WT or 5 *Igha*$^{-/-}$ mice at steady state. Asterisks indicate highly differentially expressed genes discussed in the text. The scale bar shows color coding (blue, white, red) for z-score. (**C**) Absolute numbers of PD-1^{+}CD4^{+} (top) or PD-1^{+}CD8^{+} (bottom) total (left) or antigen-experienced CD44^{+} (right) T cells from the spleen of 14 WT or *Igha*$^{-/-}$ mice determined by flow cytometry. (**D**) PD-L1-expression (MFI, mean fluorescence intensity) on splenic MZ B cells, FO B cells, total B-1 cells, B-1a cells, and B-1b cells from 5 WT or 6 *Igha*$^{-/-}$ mice. (**E**) ELISA of serum IgG1 to PPS 14, 21, 28, 56 and 86 days following i.p. immunization with Prevnar13 of 8 WT or *Igha*$^{-/-}$ mice treated with anti-PD-1 mAb and of 7 WT or 8 *Igha-/-* mice treated with control isotype-matched mAb. Mice received 200 μg i.p. of either anti-PD-1 or control mAb one day prior to immunization and one day after immunization, followed by injections every third day through day 19 post-immunization. Results summarize one (A-C, E) or two (D) independent experiments or show one experiment representative of two (F). Data are presented with mean GSVA score and 95% confidence interval (B) or mean (A, E), median (D), or mean and s.e.m (F). Significance was determined using limma modeling (B) or Mann-Whitney test (A, D-F). *p < 0.05, **p < 0.01, ***p < 0.005, ****p < 0.001.

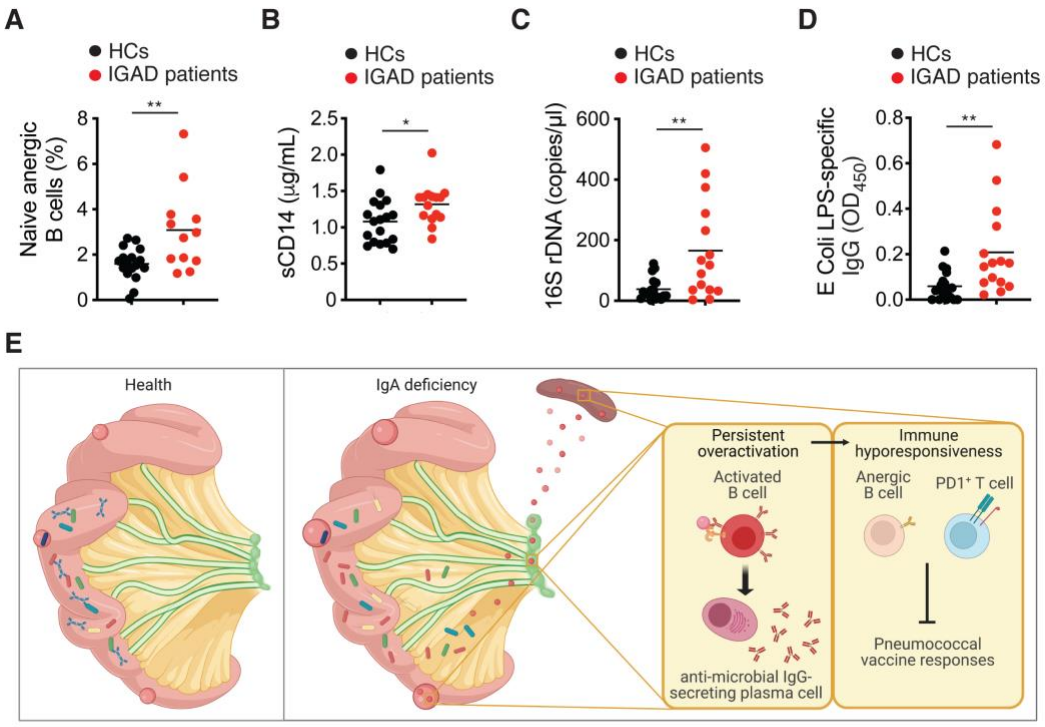

Fig. 6. IgA constrains the systemic translocation of gut commensal antigens. (**A**) Frequency (%) of circulating B cells with hyporesponsive-anergic $IgM^{lo}CD21^{lo}$ phenotype within total $IgD^{+}CD27^{-}$ naïve B cells population from 17 healthy controls (HCs) and 12 IGAD patients. (**B**) ELISA of sCD14 in serum from 18 HCs and 15 IGAD patients. (**C**) Quantitative PCR of bacterial 16S rDNA in serum from 18 HCs and 15 IGAD patients. (**D**) ELISA of IgG to LPS from *Escherichia coli* in serum from 18 HCs and 15 IGAD patients. (**E**) Proposed model depicting the impact of gut IgA on systemic IgG responses to pneumococcal vaccines. Compared to the IgA-sufficient gut (left), the IgA-deficient gut (right) experiences increased penetration of viable gut commensals into the MAT due to the defective immune exclusion of intraluminal bacteria. The resulting peripheral penetration of soluble commensal antigens from MAT-based bacteria starts at an early age and leads to the chronic stimulation of the immune system, including B and T cells. B cells release progressively increasing amounts of IgG to gut

commensal antigens (left inset), whereas T cells up-regulate PD-1 expression (right inset), respectively. Persistent nonspecific B cell stimulation by gut antigens combined with enhanced B cell-inhibitory signals from PD-1 cause the functional exhaustion of systemic B cells, which become hyporesponsive to neo-antigens from pneumococcal vaccines. Additional factors such as the depletion of B cell-stimulating signals from metabolites emerging from the IgA-coated gut microbiota (not shown) might contribute to the impairment of IgG responses to pneumococcal vaccines. Results summarize one experiment with multiple biological replicates. Data are presented with mean and significance determined using Mann-Whitney test. *$p < 0.05$, **$p < 0.01$.